Preprint typeset in JHEP style - PAPER VERSION

Cavendish–HEP–09/20

Double Parton Distributions Incorporating Perturbative QCD Evolution and Momentum and Quark Number Sum Rules

Jonathan R. Gaunt[1] **and W. James Stirling**[1,2]

[1] *Cavendish Laboratory, University of Cambridge, J.J. Thomson Avenue, Cambridge CB3 0HE, U.K.*

[2] *Department of Physics and Institute for Particle Physics Phenomenology, University of Durham, DH1 3LE, U.K.*

Abstract: It is anticipated that hard double parton scatterings will occur frequently in the collisions of the LHC, producing interesting signals and significant backgrounds to certain single scattering processes. For double scattering processes in which the same hard scale $t = \ln(Q^2)$ is involved in both collisions, we require the double parton distributions (dPDFs) $D_h^{j_1 j_2}(x_1, x_2; t)$ in order to make theoretical predictions of their rates and properties. We describe the development of a new set of leading order dPDFs that represents an improvement on approaches used previously. First, we derive momentum and number sum rules that the dPDFs must satisfy. The fact that these must be obeyed at any scale is used to construct improved dPDFs at the input scale Q_0, for a particular choice of input scale ($Q_0^2 = 1$ GeV^2) and corresponding single PDFs (the MSTW2008LO set). We then describe a novel program which uses a direct $x-$space method to numerically integrate the LO DGLAP equation for the dPDFs, and which may be used to evolve the input dPDFs to any other scale. This program has been used along with the improved input dPDFs to produce a set of publicly available dPDF grids covering the ranges $10^{-6} < x_1 < 1$, $10^{-6} < x_2 < 1$, and $1 < Q^2 < 10^9$ GeV^2.

Keywords: QCD Phenomenology, Parton Model, Hadronic Colliders.

Contents

1. Introduction

In the standard framework for calculating inclusive cross sections for hard scattering processes in hadron-hadron collisions, it is assumed that only one hard interaction occurs per collision (plus multiple soft interactions). This assumption is typically justified on the grounds that the probability of a hard parton-parton interaction in a collision is very small. Thus the probability of having two or more hard interactions in a collision is highly suppressed with respect to the single interaction probability.

Hadron-hadron collisions in which two (or more) distinct pairs of partons hard scatter are nevertheless possible. Early theoretical studies of double scattering were carried out in the context of the parton model [1–3] , with subsequent extension to perturbative QCD [4–16] . Such processes have in fact been observed experimentally – both in $\sqrt{s} = 63$ GeV pp collisions by the AFS collaboration at the CERN ISR [17] and more recently in $\sqrt{s} = 1.8$ TeV $p\bar{p}$ collisions by the CDF collaboration [18] and $\sqrt{s} = 1.96$ TeV $p\bar{p}$ collisions by the D0 collaboration [19] at the Fermilab Tevatron.

The much greater energy and higher luminosity of the LHC implies that we will observe a greater rate of events containing multiple hard interactions in this experiment than in either of the two mentioned above. Moreover, a number of calculations [20–23] suggest that the products from multiple interactions will represent an important background to signals from the Higgs and other interesting processes. Further calculations [24–26] indicate that certain types of multiple interactions will have distinctive signatures at the LHC, facilitating a detailed study of this process by the experiment.

The importance of multiple scattering signals and backgrounds at the LHC necessitates a good quantitative understanding of these processes. In particular, it is important to understand double scattering, which will be the dominant multiple scattering mode at the LHC. Assuming only the factorisation of the two hard subprocesses A and B, the cross section for this process in proton-proton scattering may be written as:

$$\sigma^D_{(A,B)} = \frac{m}{2} \sum_{i,j,k,l} \int \Gamma_{ij}(x_1, x_2, b; t_1, t_2) \hat{\sigma}^A_{ik}(x_1, x_1') \hat{\sigma}^B_{jl}(x_2, x_2') \times \Gamma_{kl}(x_1', x_2', b; t_1, t_2) dx_1 dx_2 dx_1' dx_2' d^2b \tag{1.1}$$

The $\hat{\sigma}$s are the parton-level subprocess cross sections. These are also encountered in single scattering, and are known for essentially all processes of phenomenological interest. The quantity m is a symmetry factor that equals 1 if $A = B$ and 2 otherwise. The $\Gamma_{ij}(x_1, x_2, b; t_1, t_2)$ represent generalised double distributions. They may be loosely interpreted as the inclusive probability distributions to find a parton i with longitudinal momentum fraction x_1 at scale $t_1 \equiv \ln(Q_1^2)$ in the proton, in addition to a parton j with longitudinal momentum fraction x_2 at scale $t_2 \equiv \ln(Q_2^2)$, with the two partons separated by a transverse distance b. The scale t_1 is given by the characteristic scale of subprocess A, whilst t_2 is equal to the characteristic scale of subprocess B. Note that CDF and D0 have measured double scattering via the $\gamma + 3$jet final state, with A corresponding to γ+jet production and B to dijet production.

It is typically assumed that $\Gamma_{ij}(x_1, x_2, b; t_1, t_2)$ may be decomposed in terms of longitudinal and transverse components as follows:

$$\Gamma_{ij}(x_1, x_2, b; t_1, t_2) = D_h^{ij}(x_1, x_2; t_1, t_2) F_j^i(b) \tag{1.2}$$

The function $D_h^{ij}(x_1, x_2; t_1, t_2)$ has a rigorous interpretation in leading order (LO) perturbative QCD as the inclusive probability of finding a parton i with momentum fraction x_1 at scale t_1 and a parton j with momentum fraction x_2 at scale t_2 in the proton. Accurate prediction of double parton scattering cross sections and event signatures requires good modelling of $D_h^{ij}(x_1, x_2; t_1, t_2)$ and $F_j^i(b)$. In particular, one must correctly take account of the effects of correlations in both longitudinal momenta and transverse positions in these functions.

Correlations between the partons in transverse space are highly significant – at the very least, they must tie the two partons together within the same hadron. As one might suspect, their precise calculation is not possible using perturbation theory. Existing models typically use Gaussian or exponential forms to describe the $F_j^i(b)$, or a sum of Gaussian/exponential terms [27, 28].

On the other hand, correlations in longitudinal momenta are typically ignored. The usual assumption (applied in the phenomenological calculations of [20–26]) is that at least for small x_i values the longitudinal momenta correlations are small, and therefore $D_h^{ij}(x_1, x_2; t_1, t_2)$ may be taken to be equal to a product of the relevant single parton distribution functions (sPDFs) – i.e. $D_h^{ij}(x_1, x_2; t_1, t_2) = D_h^i(x_1; t_1) D_h^j(x_2; t_2)$. With this assumption, plus the assumption that $F_j^i(b)$ is the same for all parton pairs ij involved in the double scattering process of interest, the cross section $\sigma_{(A,B)}^D$ has the particularly simple form:

$$\begin{aligned} \sigma_{(A,B)}^D &= \frac{m}{2} \frac{\sigma_{(A)}^S \sigma_{(B)}^S}{\sigma_{\text{eff}}} \\ \sigma_{\text{eff}} &= \left[\int d^2b (F(b))^2 \right]^{-1} \end{aligned} \tag{1.3}$$

The quantity $\sigma_{(X)}^S$ is the single scattering cross section for hard process X. The factor σ_{eff} in the denominator has the dimensions of a cross section. It can be understood as follows. Given that one hard scattering occurs, the probability of the other hard scattering is proportional to the flux of accompanying partons; these are confined to the colliding protons, and therefore their flux should be inversely proportional to the area (cross section) of a proton. Interestingly, the CDF and D0 measurements give $\sigma_{\text{eff}} \sim 15$ mb, which is roughly 20% of the total (elastic + inelastic) $p\bar{p}$ cross section at the Tevatron collider energy.

It is argued that the approximation of the $D_h^{ij}(x_1, x_2; t_1, t_2)$ as a product of single PDFs should be particularly applicable in collider experiments where small x values are probed (i.e. large total system centre of mass energy with respect to subprocess energy) due to the large population of partons at these x values. The CDF experimental data also agree with this assumption, with no sign of x-dependence in their measured σ_{eff} over the

x ranges accessible to them ($0.01 - 0.40$ for their first subprocess, and $0.002 - 0.20$ for the other) [29]. The D0 data confirm this result, with no measured variation of $\sigma_{\rm eff}$ with the (second highest) jet transverse momentum.

Even if the factorisation assumption holds at the CDF scale (i.e. $Q^2 \sim 100{-}1000$ GeV^2), it is unlikely that it will hold at higher scales such as will be encountered at the LHC. In [30, 31], the behaviour of the distributions $D_h^{ij}(x_1, x_2; t) \equiv D_h^{ij}(x_1, x_2; t, t)$ with the two hard scales set equal (hereafter known as the dPDFs) were investigated. The authors derived an equation dictating the scaling violations (i.e. t dependence) of the dPDFs. This equation is an analogue of the DGLAP equation for sPDFs (sDGLAP equation) [32–35]. An important prediction of this equation is that, even if the dPDFs factorise at some scale t_0, then at *any* different scale factorisation will be violated [36]. In other words, the naive product $D_h^i(x_1; t)D_h^j(x_2; t)$ where the D_h^is satisfy sDGLAP is *not* a solution of the dDGLAP equations. Explicit numerical solutions of the LO 'double DGLAP' (dDGLAP) equation based on factorised inputs at $Q_0^2 \sim 1$ GeV^2 suggest that the violations are significant even for small x, with deviations on the order of $10 - 30\%$ at $x_1 = x_2 \sim 0.1, Q^2 \sim 10^4$ GeV^2 [37, 38]. Another problem with the factorisation hypothesis is that it is inconsistent with various (number and momentum) sum rules that relate the dPDFs to the sPDFs, see Section 3.1 below.

For the purposes of the accurate prediction of double parton scattering cross sections and signals at the LHC, there is a need for a more theoretically sound set of double distributions than the naive factorised forms traditionally used. Here, we have attempted to address this issue for the specific case of the dPDFs (with $t_1 = t_2$). First, we derive sum rules corresponding to momentum and valence quark number conservation that the dPDFs must satisfy. These are used as an aid to construct 'improved' dPDFs at the scale $Q_0 = 1$ GeV that correspond to the MSTW2008LO sPDF inputs [39]. The low scale dPDFs are then used as an input in a program we have written which numerically integrates the LO dDGLAP equation to higher scales. The end products of this paper are a set of LO dPDF grids covering the ranges $10^{-6} < x_1 < 1$, $10^{-6} < x_2 < 1$, $1 < Q^2 < 10^9$ GeV^2, and all possibilities for the parton indices i and j. These grids, in addition to a simple interpolation subroutine designed to extract from the grids a dPDF value at a given x_1, x_2 and Q, can be found at Ref. [40].

This paper is organised as follows. We begin with a brief review of the dDGLAP equation in Section 2. The dPDF sum rules are introduced and discussed in Section 3, where we also explain how we have used these rules to construct input dPDFs at $Q_0 = 1$ GeV corresponding to the MSTW2008LO sPDF inputs. In Section 4, the details of the numerical procedure designed to evolve the input distributions to higher scales using the LO dDGLAP equation are given. Section 5 examines the ways in which our dPDFs differ from those obtained using previous approaches. Finally, we conclude in Section 6 with a summary and discussion of potential future directions for the work.

2. The Double DGLAP Equation

It is well established that in QCD, the parton content of the proton that is observed by

a hard probe with virtuality Q^2 (or more than one hard probe with this virtuality) is dependent on the size of the virtuality. This dependence is explained by the fact that a harder probe (with a shorter associated wavelength) is able to 'see' finer scale structure in the proton, and in particular is able to resolve parton splittings that were unresolvable using a lower $t \equiv \ln(Q^2)$ probe. This implies that parton distributions must be dependent on the scale t at which the proton is probed. There is a shift of these distributions towards smaller x values as t increases, as a consequence of a greater number of splittings being resolved.

One can visualise the change in parton distributions as one probes at steadily higher scales t than the low scale t_0 as a spacelike branching process originating from the initial distributions at scale t_0. As one probes to higher scales, one effectively progresses further in the branching process.

The dDGLAP equation is a renormalisation group equation describing the change of the dPDFs with the hard scale t. It is based on the leading logarithm approximation (LLA) of perturbative QCD (the same is true for the sDGLAP equation). This approximation corresponds to a picture of the spacelike parton branching process from the low scale t_0 to the probe scale t in which gluon emissions along the parton branches are strongly ordered in transverse momentum. Gluons emitted 'earlier' in the branching process are restricted to have smaller transverse momenta than those emitted closer to the probe scale. The dDGLAP equation effectively resums leading powers of $[\alpha_s t]^n$ generated by these gluon emissions to give the dPDFs at scale t.

In [30, 31], the following form for the dDGLAP equation is derived:

$$\begin{aligned}\frac{dD_h^{j_1 j_2}(x_1, x_2; t)}{dt} = \frac{\alpha_s(t)}{2\pi}\Bigg[&\sum_{j_1'}\int_{x_1}^{1-x_2}\frac{dx_1'}{x_1'}D_h^{j_1' j_2}(x_1', x_2; t)P_{j_1'\to j_1}\left(\frac{x_1}{x_1'}\right)\\ &+\sum_{j_2'}\int_{x_2}^{1-x_1}\frac{dx_2'}{x_2'}D_h^{j_1 j_2'}(x_1, x_2'; t)P_{j_2'\to j_2}\left(\frac{x_2}{x_2'}\right)\\ &+\sum_{j'}D_h^{j'}(x_1+x_2; t)\frac{1}{x_1+x_2}P_{j'\to j_1 j_2}\left(\frac{x_1}{x_1+x_2}\right)\Bigg]\end{aligned} \tag{2.1}$$

In addition to the dPDFs and sPDFs $D_h^j(x;t)$, the equation (2.1) contains two different types of splitting functions. The first are the well-known splitting functions $P_{i\to j}(x)$ previously encountered in the context of the sDGLAP equation. They are given to both LO and NLO in [41]. The second, the $P_{i\to jk}(x)$, are new. At leading order, the function $P_{i\to j}(x)$ may be interpreted as the probability of a parton i splitting to give a parton j with a fraction x of the longitudinal momentum of the parent parton and a transverse momentum squared much smaller than Q^2 (where $t \equiv \ln(Q^2)$) [35]. The function $P_{i\to jk}(x)$ may be interpreted at LO as the probability of a parton i splitting to give the two partons j and k, the first of which has a fraction x of the linear momentum of the parent parton, the second of which has the remainder of the linear momentum $1-x$, and both of which have transverse momentum squared much less than Q^2.

The splitting functions $P_{i\to i}(x)$ each possess a large negative contribution at $x = 1$ (these are contained within the 'plus prescription' functions together with explicit delta functions in the definitions). This contribution is included to take account of the fact that splittings of the parton i into other partons with lower momentum act to reduce the population of partons with the original momentum. At a fundamental level, the contributions at $x = 1$ result from virtual gluon radiation diagrams.

On the other hand, the functions $P_{i\to jk}(x)$ do not contain such contributions. This is to be expected as a virtual process is clearly not able to achieve the $1 \to 2$ splitting $i \to jk$. At LO, the function $P_{i\to jk}(x)$ is related to the 'real splitting' part[1] of the normal splitting functions $P^R_{i\to j}(x)$ according to:

$$P^R_{i\to j}(x) = \sum_k P_{i\to jk}(x) \tag{2.2}$$

Equation (2.2) is the simple statement that the probability of splitting $i \to j + anything$ is equal to the sum of probabilities of splitting $i \to j + k$, summed over all possibilities for k.

A further simplification to (2.2) is possible at LO. Due to the fact that QCD only allows certain types of three particle vertices (i.e. triple gluon vertices and 'gluon emission from a quark' type vertices), the LO $P_{i\to jk}(x)$ is only nonzero for a small number of $\{i, j, k\}$ combinations. In fact, given i and j, there exists at most one choice for k which makes $P_{i\to jk}(x)$ nonzero. We shall denote this special value of k by $\kappa(i, j)$. For example, $\kappa(i, j)$ is g when $i = q_i, j = q_i$, and $\bar{q}_i$ when $i = g, j = q_i$.

Given this fact, we note that (2.2) must contain at most only one term on the right hand side, and we may write:

$$P^R_{i\to j}(x) = P_{i\to j\kappa(i,j)}(x) \tag{2.3}$$

In (2.3), we have extended the definition of $\kappa(i, j)$ to cases where there exists no choice for k to make $P_{i\to jk}(x)$ nonzero. In these cases, $\kappa(i, j)$ can be chosen to be any parton, as both the right and left hand sides are zero for any choice.

Equation (2.3) effectively defines $P_{i\to jk}$ for all cases in which it is nonzero. At LO then, we may construct the following definition for $P_{i\to jk}$:

$$P_{i\to jk}(x) = \begin{cases} P^R_{i\to j}(x) & \text{if } k = \kappa(i, j) \\ 0 & \text{otherwise} \end{cases} \tag{2.4}$$

It is interesting to consider the generalisation of the $P_{i\to jk}(x)$ functions to NLO (and indeed higher orders). Here one encounters a problem, in that the function $P_{i\to jk}(x)$ only has one longitudinal momentum argument because it is assumed that the parton k must possess the remaining longitudinal momentum originally carried by i that was not given to j, i.e. $1 - x$. This is certainly true at leading order, where only two partons can be

[1]The functions $P^R_{i\to j}(x)$ are obtained from the functions $P_{i\to j}(x)$ by dropping the terms proportional to $\delta(1 - x)$. This includes removing plus prescription + signs where they appear.

produced in a single splitting, by conservation of momentum. However, it is not true in general at NLO, where a single splitting can contain two QCD vertices, and produce three partons. At NLO and above, the splitting function $P_{i\to jk}$ should have two arguments, x_1 and x_2.

The expansion of the more general function $P_{i\to jk}(x_1, x_2)$ in terms of powers of α_s would read as follows:

$$P_{i\to jk}(x_1, x_2) = \delta(1 - x_1 - x_2)P^{(0)}_{i\to jk}(x_1) + \frac{\alpha_s}{2\pi}P^{(1)}_{i\to jk}(x_1, x_2) + \dots \tag{2.5}$$

The higher-order coefficients in this expansion cannot be obtained trivially from the higher-order coefficients of the splitting function $P_{i\to j}(x)$ as in the LO case. The general relation between the two for $x < 1$ is:

$$P^{(n)}_{i\to j}(x_1) = \sum_k \int_0^{1-x_1} dx_2 \; P^{(n)}_{i\to jk}(x_1, x_2) \tag{2.6}$$

The unintegrated $P^{(n)}_{i\to jk}(x_1, x_2)$ must contain more information than the $P^{(n)}_{i\to j}(x)$ for $n > 0$, and hence cannot be obtained from them.

A consequence of the fact that $P_{i\to jk}(x)$ with a single longitudinal momentum argument x is not the right function to use at NLO and above is that the precise structure of the dDGLAP equation given in (2.1) can only be applicable at LO.[2] In what follows we restrict our analysis to the LO case, but will return to the generalisation of (2.1) to NLO in a future study.

One can interpret the terms on the right-hand side of (2.1) using the parton branching picture.[3] Consider the inclusive probability of finding a pair of partons in the proton with flavours j_1 and j_2 and longitudinal momentum fractions between x_1 and $x_1+\delta x_1$ and x_2 and $x_2+\delta x_2$ respectively at scale t, $D_h^{j_1 j_2}(x_1, x_2; t)\delta x_1 \delta x_2$. It is obvious that when t is increased to $t + \Delta t$, two types of process may contribute to the change in this quantity. Splittings from higher-momentum partons giving rise to $j_1 j_2$ pairs with the correct momentum act to increase this quantity, whilst splittings within the $j_1 j_2$ pairs to give partons of lower momentum act to decrease the quantity.

At leading order in α_s (which, as we have established, is the order under which equation (2.1) was derived), there are three types of splitting process that give rise to a pair of partons $j_1 j_2$ with momenta in the ranges $x_1 \to x_1 + \delta x_1$, $x_2 \to x_2 + \delta x_2$. The three are drawn schematically in Fig. 1.

In the first, we start with a pair of partons $j_1' j_2$ with momenta in the ranges $x_1' \to x_1' + \delta x_1'$, $x_2 \to x_2 + \delta x_2$. The quantity x_1' must satisfy $x_1 < x_1' < 1 - x_2$ – i.e. be large enough that j_1' can split to give j_1, and be small enough that the initial pair of partons is not carrying more momentum than the proton they are in. The parton j_1' then splits to give as one of the products a j_1 with momentum in the range $x_1 \to x_1 + \delta x_1$. The second process is very similar but involves a splitting in the second parton. The third involves a

[2] This is not explicitly stated in [30, 31].

[3] We use similar arguments as are used in Section 5.2 of [41] to explain the terms on the right hand side of the sDGLAP equation.

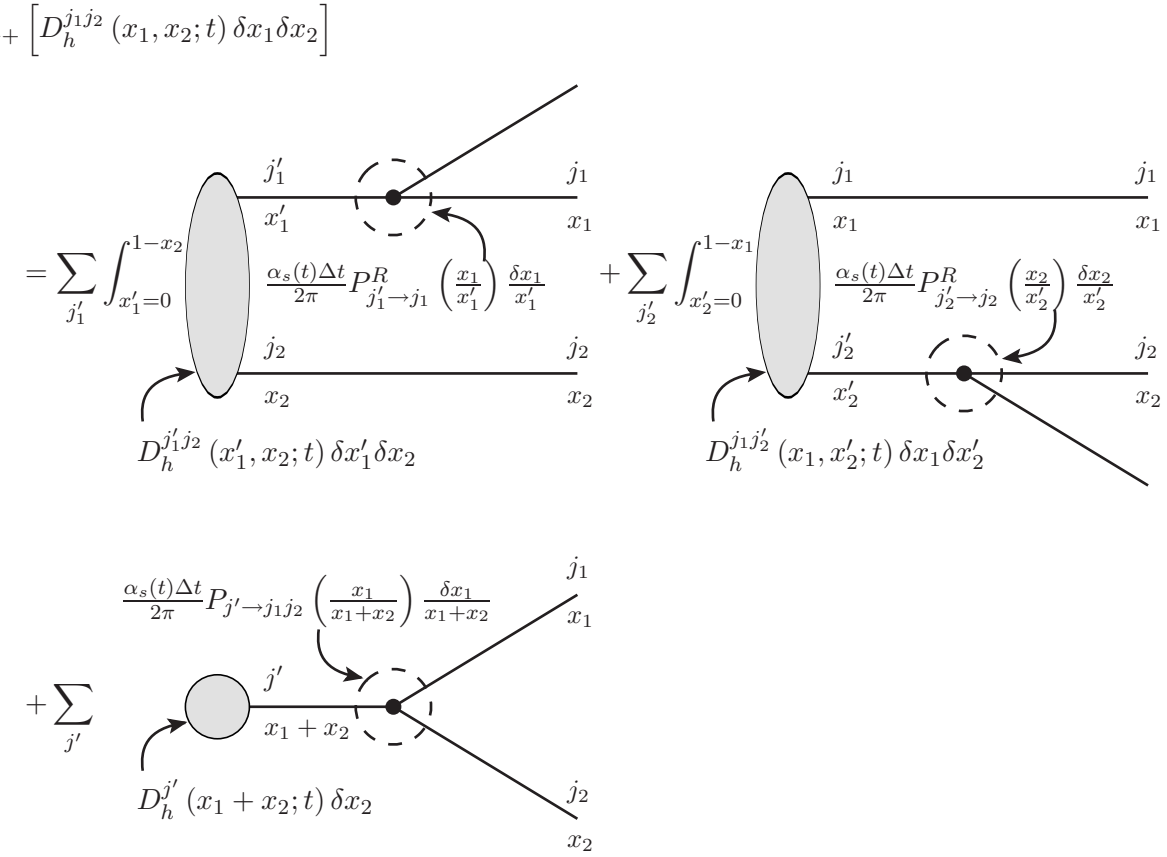

Figure 1: Splitting processes that increase the population of $j_1 j_2$ parton pairs with momenta in the ranges $x_1 \to x_1 + \delta x_1$, $x_2 \to x_2 + \delta x_2$. $P^R_{i \to j}(x)$ is the 'real splitting' part of the splitting function $P_{i \to j}(x)$ – i.e. the splitting function minus the terms proportional to $\delta(1-x)$.

single parton j' with just the right momentum $x_1 + x_2 \to x_1 + x_2 + \delta x_2$ splitting to give as its two daughters the pair $j_1 j_2$ with momenta in the appropriate ranges.

The leading order splitting processes reducing the population of $j_1 j_2$ partons with momenta in the given ranges are given in Fig. 2. There are two processes – in the first, the j_1 parton splits to give lower momentum partons, whilst in the second the j_2 splits.

The correspondence between the diagrams of Figs. 1 and 2 representing the splitting processes and the terms on the RHS of (2.1) is fairly clear. Suitable labels have been added to the figures to bring out this correspondence. It is important to note that the first two sets of terms on the RHS of (2.1) cover four diagrams – the first two of both Fig. 1 and Fig. 2. The 'real splitting' parts of the terms correspond to the diagrams in Fig. 1, whilst the 'virtual correction' parts correspond to the diagrams in Fig. 2. We also note that the last set of terms on the RHS of (2.1) contains sPDFs because it corresponds to the diagram in which a *single* parton splits to give the pair $j_1 j_2$. There is no integral in these terms because of the property of LO QCD that a single splitting can only give rise to two partons. Thus the single parton that splits is essentially restricted to have momentum exactly equal to $x_1 + x_2$. We shall hereafter refer to the last set of terms on the RHS of

$\Delta_- \left[D_h^{j_1 j_2}(x_1, x_2; t)\, \delta x_1 \delta x_2 \right]$

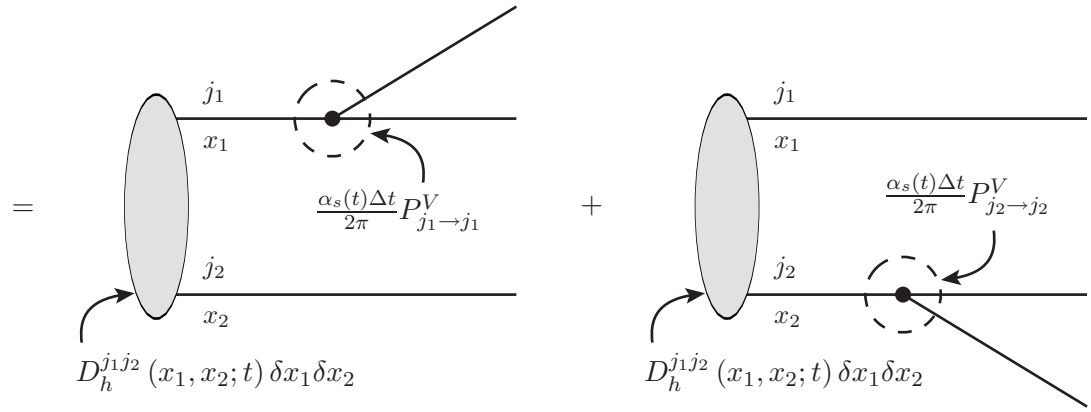

Figure 2: Splitting processes that decrease the population of $j_1 j_2$ parton pairs with momenta in the ranges $x_1 \to x_1 + \delta x_1$, $x_2 \to x_2 + \delta x_2$. $P^V_{j \to j}$ is equal to the sum of the coefficients of the $\delta(1-x)$ terms in the splitting function $P_{j \to j}(x)$ (including $\delta(1-x)$ terms contained within plus prescription functions).

(2.1) as the 'sPDF feed' terms, for obvious reasons.

A solution to (2.1) in terms of sPDFs is obtained in [30, 31], and presented for the first time in x-space in [36]. Let us introduce the 'natural' evolution variable τ defined in terms of t according to:

$$\begin{aligned} \tau &= \int_{t_0}^{t} dt' \frac{\alpha_s(t')}{2\pi} \\ &= \frac{1}{2\pi b} \ln \left[\frac{t - \ln(\Lambda^2_{QCD})}{t_0 - \ln(\Lambda^2_{QCD})} \right] \text{ at LO} \end{aligned} \tag{2.7}$$

In terms of the variable τ, the solution to the dDGLAP equation reads:

$$\begin{aligned} D_h^{j_1 j_2}(x_1, x_2; \tau) &= D^{j_1 j_2}_{h(corr)}(x_1, x_2; \tau) \\ &+ \sum_{j'_1 j'_2} \int_{x_1}^{1-x_2} \frac{dz_1}{z_1} \int_{x_2}^{1-z_1} \frac{dz_2}{z_2} D_h^{j'_1 j'_2}(z_1, z_2; \tau = 0) \\ &\times D^{j_1}_{j'_1}\left(\frac{x_1}{z_1}; \tau\right) D^{j_2}_{j'_2}\left(\frac{x_2}{z_2}; \tau\right) \end{aligned} \tag{2.8}$$

where:

$$\begin{aligned} D^{j_1 j_2}_{h(corr)}(x_1, x_2; \tau) = \sum_{j' j'_1 j'_2} \int_0^{\tau} d\tau' \int_{x_1}^{1-x_2} \frac{dz_1}{z_1} \int_{x_2}^{1-z_1} \frac{dz_2}{z_2} D_h^{j'}(z_1 + z_2; \tau') \\ \times \frac{1}{z_1 + z_2} P_{j' \to j'_1 j'_2}\left(\frac{z_1}{z_1 + z_2}\right) D^{j_1}_{j'_1}\left(\frac{x_1}{z_1}; \tau - \tau'\right) D^{j_2}_{j'_2}\left(\frac{x_2}{z_2}; \tau - \tau'\right) \end{aligned} \tag{2.9}$$

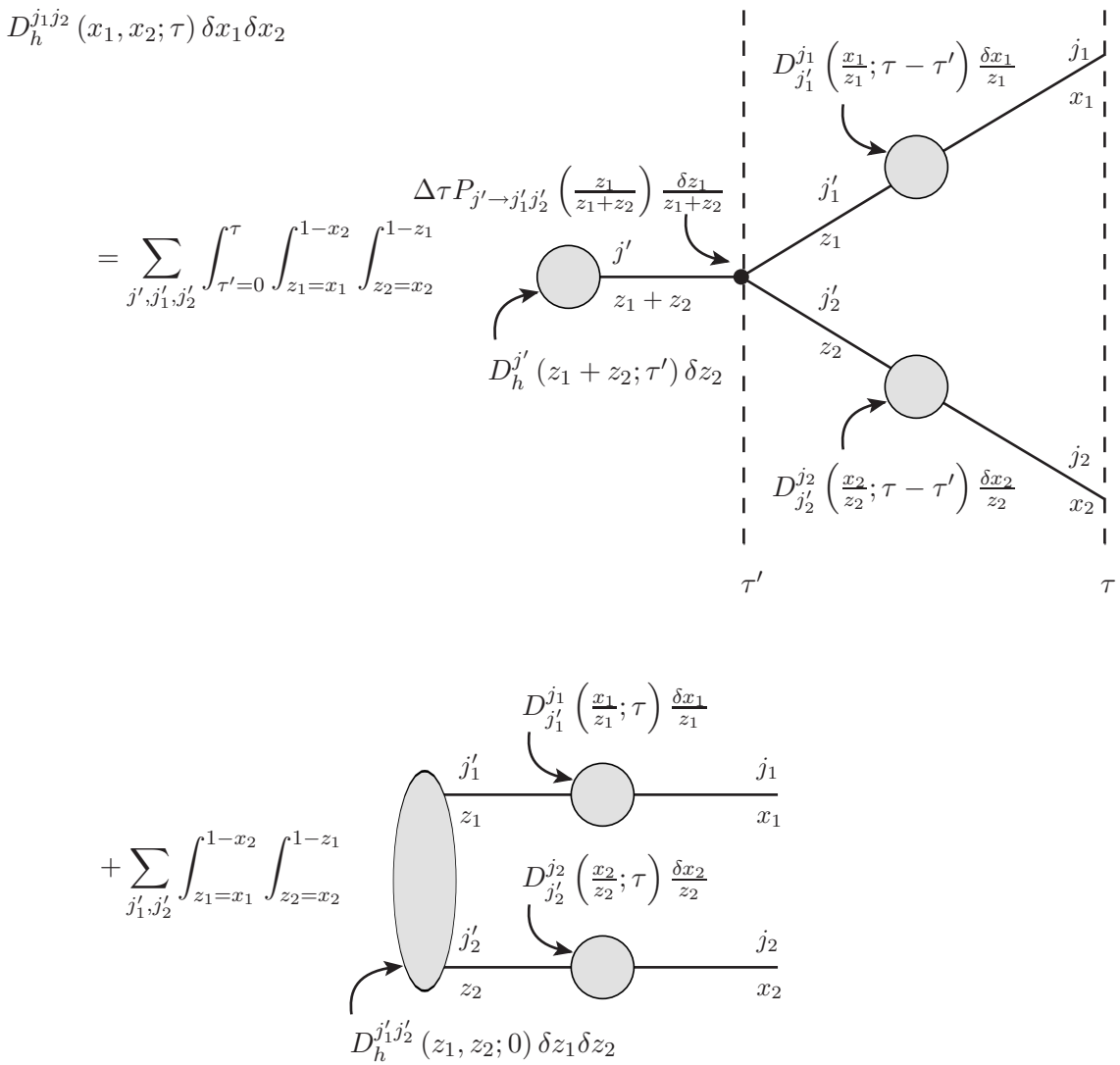

Figure 3: A schematic representation of the solution of the dDGLAP equation (2.8) in terms of the parton branching picture.

The Green's functions $D_i^j(x;\tau)$ are defined such that they satisfy the initial conditions $D_i^j(x;\tau=0) = \delta_{ij}\delta(1-x)$ and change with τ according to the sDGLAP equation:

$$\frac{dD_i^j(x;\tau)}{d\tau} = \sum_{j'} \int_x^1 \frac{dz}{z} D_i^{j'}(z;\tau) P_{j' \to j}(x/z) \tag{2.10}$$

In effect, the function $D_i^j(x;\tau)$ gives the inclusive probability that one finds a parton j with longitudinal momentum fraction x at scale τ inside a dressed object that looks like a pure i parton at the scale $\tau = 0$.

A pictorial representation of the solution (2.8) in terms of parton branching is given in Fig. 3. One observes the need to specify some initial conditions $D_h^{j_1' j_2'}(x_1, x_2; \tau = 0)$ to obtain the distributions at higher scale, which is a direct reflection of the fact that the

dDGLAP equation can only predict changes in the distributions with τ.

The depiction of dDGLAP evolution as in Fig. 3 leads us to make a suggestion as to how one might calculate the double distributions for which the two scales are not equal, $D_h^{ij}(x_1, x_2; \tau_1, \tau_2)$. Consider the analogous figure to Fig. 3 for these distributions. It seems likely that this figure would be the same, except with τ_1 replacing τ on the 'upper legs' of the diagrams, τ_2 replacing τ on the 'lower legs' of the diagrams, and the upper limit of the τ' integration replaced by $\min(\tau_1, \tau_2)$. If this ansatz is correct, the double distributions $D_h^{ij}(x_1, x_2; \tau_1, \tau_2)$ with (say) $\tau_1 < \tau_2$ should be calculated by taking the dPDFs with $\tau = \tau_1$, and then performing sDGLAP evolution at each x_1 from τ_1 to τ_2 in the x_2 variable. The upper limit in the sDGLAP evolution at given x_1 should be $1 - x_1$.

3. The Double Parton Sum Rules and the Initial Distributions

3.1 The Double Parton Sum Rules

It is well known that the sPDFs satisfy two types of sum rules which represent the fact that both momentum and valence quark number should be conserved under evolution. One might wonder whether corresponding rules exist for the dPDFs. It is straightforward to show from the dDGLAP evolution equation (2.1) that *if* the following equalities hold at the starting scale t_0, then LO DGLAP evolution will result in them being preserved at any other scale t:

Momentum Sum Rule:
Let M be the momentum fraction carried by the proton (= 1). Then:

$$\sum_{j_1} \int_0^{1-x_2} dx_1 x_1 D_h^{j_1 j_2}(x_1, x_2; t) = (M - x_2) D_h^{j_2}(x_2; t) \tag{3.1}$$

Number Sum Rule:
Let $j_{1v} \equiv j_1 - \overline{j}_1$ ($j_1 \neq g$), and $N_{j_{1v}}$ be the number of 'valence' j_1 quarks in the proton. Then:

$$\int_0^{1-x_2} dx_1 D_h^{j_{1v} j_2}(x_1, x_2; t) = \begin{cases} N_{j_{1v}} D_h^{j_2}(x_2; t) & \text{when } j_2 \neq j_1 \text{ or } \overline{j}_1 \\ (N_{j_{1v}} - 1) D_h^{j_2}(x_2; t) & \text{when } j_2 = j_1 \\ (N_{j_{1v}} + 1) D_h^{j_2}(x_2; t) & \text{when } j_2 = \overline{j}_1 \end{cases} \tag{3.2}$$

These sum rules are the analogue of the result in probability theory that for two continuous random variables X and Y, the probability density functions relating to X and Y must satisfy:

$$\int dx x^a f(X = x \cap Y = y) = E(X^a \mid Y = y) f(Y = y) \tag{3.3}$$

The integral is performed over all values that X can take given that $Y = y$, and $E(X^a \mid Y = y)$ is the expectation value of X^a given that Y has value y. The presence

of the $E(X^a \mid Y = y)$ is crucial and explains all the prefactors on the right hand sides of Eqns. (3.1) and (3.2). Given that we have found a parton with flavour j_2 and longitudinal momentum fraction x_2, the fractional momentum carried by all of the other partons must add up to $(1 - x_2)$ – hence this prefactor on the right hand side of (3.1). Given that we have found a parton with flavour j_1, the number of j_1 partons minus the number of $\bar{j}_1$ partons elsewhere in the proton must be equal to $(N_{j_{1v}} - 1)$ (as we have effectively removed a j_1). The prefactors for the other number sum rule cases can be justified using similar arguments.

The fact that the forms of the number and momentum sum rules can be justified using general arguments strongly suggests that these rules should hold to all orders in perturbation theory, just as the sPDF number and momentum sum rules do. We have been restricted to an LO proof that they hold at all scales if they hold at the starting scale by the fact that we only have the LO dDGLAP equation.

Although we have not derived the momentum and number sum rules from first principles, they appear to satisfy a number of non-trivial consistency checks. For example, one might worry that there might not be a set of dPDFs that satisfy the full set of rules. A potential source of tension between the different rules is the integral:

$$\sum_{j_2} \int_0^1 dx_1 \int_0^{1-x_1} dx_2 x_2 D^{j_{1v} j_2}(x_1, x_2; t) \tag{3.4}$$

One can evaluate this integral using (3.1) or (3.2), in combination with appropriate sPDF sum rules. If different results were produced depending on which dPDF sum rule was used, this would indicate an inconsistency. However, one obtains the same result, $N_{j_{1v}} - f_{j_{1v}}$ (where $f_{j_{1v}}$ is the momentum fraction carried by valence j_1 partons), with either approach. This lends further credibility to the sum rules (3.1) and (3.2).

It is notable that the complete set of dPDF sum rules, (3.1) and (3.2), do not appear anywhere in the extant literature, although similar sum rules have been derived for the two-particle fragmentation functions in [42]. An early paper on the subject, [3] (see also [10]), introduces some 'constraints' resembling the number sum rules, which are used as an aid in constructing some simple model dPDFs. However, the constraints are only imposed for two specific dPDF cases, and the paper does not make any explicit statement about the general form of the number sum rule. In particular, they do not describe the subtleties of the number sum rule with regard to the different possible proportionality constants on the right hand side of (3.2).

In some sense, the dPDF sum rules are more restrictive than their sPDF counterparts. The sPDF sum rules state that the quantities $M \equiv \sum_i \int_0^1 dx x D_h^i(x; t)$ and $N_{i_v} \equiv \int_0^1 dx D_h^{i_v}(x; t)$ are conserved under evolution whatever their initial values, and we make the physical choices $M = 1, N_{u_v} = 2, N_{d_v} = 1$ for the proton. On the other hand, Eqns. (3.1) and (3.2) are only preserved under evolution if they hold at the starting scale. This is linked to the fact that one initially has the freedom in the sum rules to specify the momentum/parton composition of the hadron M and N_{i_v} (although $M \neq 1$ is not very physical). However, once these have been specified in the sPDF sector, the structure of the multiparton sum rules is effectively fixed.

dPDF Type	Relevant Sum Rules
Valence-Valence	Number (involved in two rules)
Valence-Sum	Number + Momentum
Valence-Tensor	Number
Tensor-Tensor	None
Tensor-Sum	Momentum
Sum-Sum	Momentum (involved in two rules)

Table 1: The different dPDF classes under the 'double evolution' representation of the dPDFs, and the types of sum rules each is engaged in.

The restrictive nature of the dPDF sum rules can be used to place nontrivial constraints on the input distributions that are physically allowable in the dDGLAP equation. If we believe that the dPDF sum rules should hold at the starting scale, then we can use the constraints provided by the rules to improve on the factorised inputs previously used at the starting scale $Q_0^2 \sim 1$ GeV^2. This is discussed in the next section.

3.2 Use of the Double Parton Sum Rules to improve the Input Distributions

As was mentioned in Section 1, it is a common assumption that the input double distributions should be equal to the product of the relevant sPDFs at low x_1 and x_2. The logic behind this is that there exist large populations of partons of all active flavour types and x values at low x. Given these large populations, we would expect the extraction of a parton with a given flavour type j_1 and small longitudinal momentum x_1 not to have a strong effect on the probability of finding another parton of flavour j_2 (where j_2 can be equal to j_1) and small longitudinal momentum x_2. This leads to a joint probability distribution which can be expressed as a product of single distributions at low x_1, x_2.

This factorisation assumption appears to be backed up by the available CDF and D0 data. Consequently, we would like our improved input dPDFs to maintain a factorised form for low x_1, x_2, whilst now obeying the sum rules (3.1) and (3.2). The first question to be addressed in this section is whether this is in fact possible for all the dPDFs, i.e. whether the sum rules are compatible with factorisation at low x_1, x_2 in all cases.

To help answer this question, we introduce the 'double evolution' representation for the dPDFs. In this representation, the well-known {singlet,gluon,valence,tensor} /$\{\Sigma, g, V_i, T_i\}$ combinations (defined in, for example, Chapter 4 of [41]) are used as the flavour basis for both parton indices in the dPDF. The use of this representation has the advantage that it splits the dPDFs into six sets, each of which must satisfy different combinations of the sum rules. We refer to the singlet and gluon combinations as the 'sum' combinations (as they describe the sum of quark and gluon contributions respectively). Since $\sum j = \Sigma + g$, any dPDF with a 'sum' flavour index will be involved in a momentum sum rule, whilst any dPDF with a 'valence' flavour index will be involved in a number sum rule. Those dPDFs where each of the indices are one out of the 'sum' and 'valence' combinations will be involved in two sum rules. The six sets of dPDFs along with the combinations of sum rules each is involved in are given in Table 1.

If one investigates each class of dPDF and their respective sum rules, then one finds that in most cases one is allowed dPDFs which satisfy the sum rules and are approximately equal to the product of single distributions at low x_1 and x_2. There is however a type of dPDF for which these two requirements cannot be simultaneously satisfied – the dPDF with two of the same valence combinations as its flavour indices (e.g. $D_h^{u_v u_v}$).

The number sum rule that this type of dPDF must satisfy reads:

$$\int_0^{1-x_2} dx_1 D_h^{j_v j_v}(x_1, x_2; t_0) = N_{j_v} D_h^{j_v}(x_2; t_0) - D_h^{j+\bar{j}}(x_2; t_0) \tag{3.5}$$

Consider this equation for small x_2. Assuming no pathological behaviour of the function $D_h^{j_v j_v}(x_1, x_2; t_0)$ near the kinematical bound $x_1 + x_2 = 1$, the integral on the left hand side of (3.5) is dominated by contributions from the small x_1 region where $D_h^{j_v j_v}(x_1, x_2; t_0)$ is largest. A factorised form for $D_h^{j_v j_v}(x_1, x_2; t_0)$ at small x_1, x_2 would then result in the left hand side behaving like $x_2^{-a_v}$ (where x^{-a_v} is the small x behaviour of a typical valence sPDF).

On the other hand, the right hand side of (3.5) is dominated by the $-D_h^{j+\bar{j}}(x_2; t_0)$ term. This is due to the fact that this term receives contributions from the sea, and sea sPDFs diverge faster than valence sPDFs at low x. We expect $-D_h^{j+\bar{j}}(x_2)$ to behave like $-x_2^{a_s}$ (where a typical sea sPDF behaves like x^{a_s} at low x). The right hand side then behaves very differently[4] from the left hand side, and it is impossible to satisfy the sum rule (3.5) using a dPDF that factorises at low x_1, x_2.

We conclude that we must abandon the possibility of factorisation into a product of sPDFs at low x_1, x_2 for the $D_h^{j_v j_v}(x_1, x_2; t_0)$. The fundamental origin of the second term on the right hand side of (3.5) which precludes the possibility of a factorised form for $D_h^{j_v j_v}(x_1, x_2; t_0)$ is of course in number effects. By 'number effects' we mean the fact that finding a parton of a given type alters the probability of finding a further parton of the same type, due to the fact that the number of that parton has decreased.

The CDF and D0 results are not in contradiction with the above conclusion, since in these experiments the vast majority of double parton scatterings observed would have been initiated by gluons and sea quarks. The dPDFs relevant to these partons are able to have factorised forms at low x_1, x_2.

At first glance, it might appear that the statement of the inadequacy of factorised forms as applied to the valence-valence distributions has already been made, in [10]. However, our statement and the one in [10] are really very different things. In [10], the authors argue that one should not use a factorised form for the valence-valence dPDFs at *large* x_1, x_2. The reasoning behind this is that the inaccuracies of the factorised ansatz at large x_1, x_2 due to the fact that it neglects momentum conservation effects are most strongly noticed in the valence-valence dPDFs, which are dominant at large x_1, x_2. Whilst we agree with their conclusions, we further propose that the factorised forms should not be used to describe equal flavour valence-valence dPDFs at *small* x_1, x_2, a point that is missed in [10] and elsewhere.

[4]Regge theory arguments, for example, would suggest $a_v \simeq \frac{1}{2}$ and $a_s \simeq 1$, and 'modern' global fit sPDFs show a similar trend.

Bearing in mind the points made above, we proceed to discuss how some input distributions approximately obeying the sum rules might be obtained. One might initially wonder whether it is possible to develop a framework for constructing dPDFs out of combinations of sPDFs that does not make reference to any specific choices for the input sPDFs (e.g. MSTW, CTEQ). Instead, it would make intelligent use of the sum rules the sPDFs have to satisfy to ensure the dPDF sum rules were satisfied. However, investigation into this route has revealed that a framework of this kind does not seem to exist, even to construct dPDFs that only satisfy one of the two types of sum rules.

Our discussion must therefore be based around some specific set of input sPDFs. For the purposes of producing the most accurate set of dPDFs we can, it would seem sensible to use the inputs from the most recent LO fit by one of the PDF fitting collaborations. We have chosen to use a set which almost exactly corresponds to the MSTW2008 LO inputs (Equations 6-12 and the first column of Table 4 in [39], with $Q_0 = 1$ GeV and $\alpha_s(Q_0) = 0.68183$). The only differences between our inputs and those of [39] are that we have set the initial s_v distribution to zero, and have added the following terms to the $\overline{d}$ distribution:

$$-148.103388x^3(1-x)^{10.8801} + 500x^4(1-x)^{10.8801} \tag{3.6}$$

These modifications have been made in order to fix the problem that the MSTW2008 LO $\overline{s}$ and $\overline{d}$ input distributions go slightly negative in some region of x. Even though strictly speaking these LO sPDFs should never go negative, the deviations below zero observed in the MSTW2008 LO $\overline{s}$ and $\overline{d}$ inputs are perhaps tolerable in single scattering calculations due to their small size ($\overline{s}, \overline{d} > -0.0005$). However, we must insist on using sPDFs which are strictly non-negative when expressed in the 'human' flavour basis[5] to build our input dPDFs. We can explain why this has to be the case by considering the dPDFs in the 'double human' basis in which at least one flavour index corresponds to an sPDF which goes negative. Like all LO dPDFs in the 'double human' basis, they cannot go negative (due to their interpretation as a probability). If we use a pseudo-factorised prescription to construct the dPDFs, then these dPDFs will go very seriously negative where the sPDF in one direction takes small negative values, and the sPDF in the other becomes large and positive. We therefore require strictly non-negative input sPDFs.

We can identify two key features that we would like to build in to our set of input dPDFs. These are the following:

1. The dPDFs should be suppressed below factorised values near the kinematical bound (i.e. the line $x_1 + x_2 = 1$) due to phase space considerations.

2. Terms should be added/subtracted from certain dPDFs to take account of number effects.

Let us begin by discussing how the first requirement might be incorporated. In the early papers [3, 5, 7, 10], a common $(1 - x_1 - x_2)$ suppression factor multiplying all of the dPDFs was advocated. This was motivated by arguments based on the recombination

[5]The 'human' flavour basis is the one in which the parton index $i = g, u, \bar{u}$, etc.

model of [43], or the Kuti-Weisskopf model of [44]. More recently [38], it has been suggested that a higher power of $(1 - x_1 - x_2)$, such as $(1 - x_1 - x_2)^2$, might be appropriate. With the benefit of knowledge of the sum rules, we can see that neither of these alternatives is entirely satisfactory. To illustrate this, let us just consider the momentum sum rule for the moment (which is the relevant rule with regards to phase space considerations), and let us consider the lines $x_1 = 0$ and $x_2 = 0$. Along these lines, all momentum sum rules are perfectly satisfied using factorised dPDFs, whilst dPDFs including a $(1 - x_1 - x_2)$ or $(1 - x_1 - x_2)^2$ factor violate the sum rules badly.

Thus a $(1-x_1-x_2)^n$ factor alone multiplying all of the dPDFs suppresses the functions rather too severely near the lines $x_1 = 0$ and $x_2 = 0$, and it would seem that a phase space factor which approached 1 near these lines would be more desirable. We can actually make sense of this from an intuitive point of view. The phase space suppression factor is inserted to take account of the fact that finding a parton with $x = x_1$ reduces the probability of finding another parton with $x = x_2$ if $x_1 + x_2$ is close to 1. One would expect a much smaller reduction if x_1 were small and x_2 were large than if both x_1 and x_2 were large, even if the sum of x_1 and x_2 was the same in both cases. Indeed, one would anticipate that the reduction should tend to zero as x_1 (or x_2) tended to zero – that is, the phase space factor should approach 1 as one approaches the lines $x_1 = 0$ and $x_2 = 0$.

Here, we continue to follow the tradition set by previous papers in that we have attempted to apply a universal phase space factor to all of the dPDFs. Use of a (positive) universal phase space factor has the advantage that it is guaranteed to produce positive double human basis dPDFs. However, instead of using $(1 - x_1 - x_2)^n$ alone, we tried the following as a 'first guess' for the phase space factor ρ, motivated by the above discussion:

$$\rho(x_1, x_2) = (1 - x_1 - x_2)^n (1 - x_1)^{-n} (1 - x_2)^{-n} \tag{3.7}$$

Following the more recent work by Korotkikh and Snigirev [38], we choose n to be 2. This choice of phase space factor gave dPDFs which satisfied the momentum sum rules reasonably well. In the left panel of Fig. 4, we plot the 'sum rule ratio' with this phase space factor for the particular example of the $(\Sigma + g)g$ momentum sum rule – the sum rule ratios for the other momentum sum rules exhibit very similar behaviour. The sum rule ratio for a particular sum rule and set of dPDFs is defined as the sum rule integral calculated using the dPDFs divided by the sPDF quantity it should be equal to. It is a function of an x variable, and measures how well the dPDFs satisfy the given sum rule – the closer the ratio is to 1 over the full x range, the better the dPDFs satisfy the sum rule.

On the other hand, the dPDF number sum rules are not particularly well satisfied by this prescription (this is illustrated in the right panel of Fig. 4). This is true even for those dPDFs which are involved in a number sum rule but which are not affected by number effects – e.g. $u_v d_v$. For these dPDFs, the phase space factor alone should be sufficient to cause the dPDFs to satisfy the relevant number sum rules – thus our first guess is not fully satisfactory. We have discovered that a slight adjustment to the form (3.7) resolves this problem. Let us allow the phase space factor to depend on the parton indices i, j on the dPDF such that (prior to adjustments relating to point 2 above) the input dPDFs are

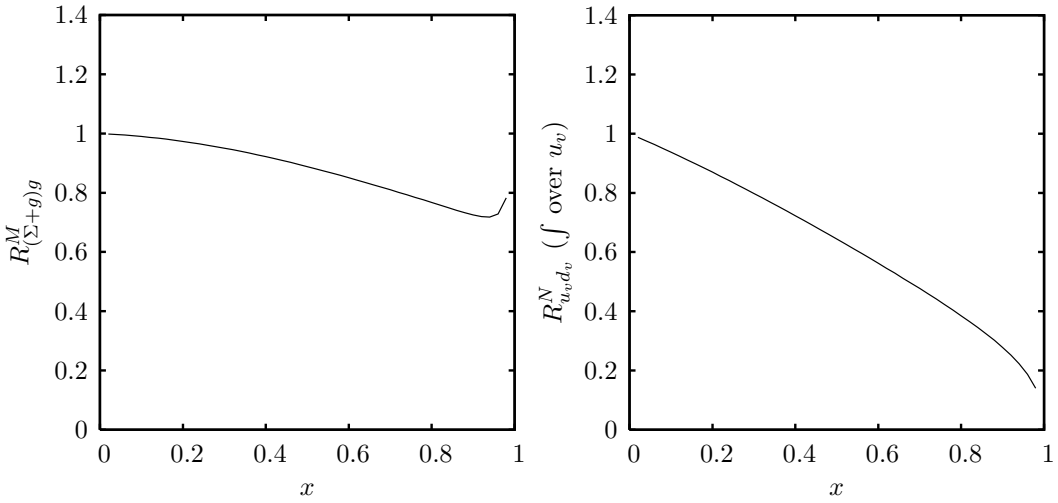

Figure 4: Sum rule ratios for the $(\Sigma + g)g$ momentum and $u_v d_v$ (integrating over u_v) number sum rules, when the phase space factor is as given in (3.7) with $n = 2$.

constructed according to:

$$D_h^{ij}(x_1, x_2; t_0) = D_h^i(x_1; t_0) D_h^j(x_2; t_0) \rho^{ij}(x_1, x_2) \tag{3.8}$$

We now define $\rho^{ij}(x_1, x_2)$ as follows:

$$\rho^{ij}(x_1, x_2) = (1 - x_1 - x_2)^2 (1 - x_1)^{-2-\alpha(j)} (1 - x_2)^{-2-\alpha(i)} \tag{3.9}$$

where:

$$\alpha(i) = \begin{cases} 0 & \text{if } i \text{ is a sea parton} \\ 0.5 & \text{if } i \text{ is a valence parton} \end{cases} \tag{3.10}$$

If either i and/or j contain both valence and sea contributions, then one should construct the dPDF by taking the factorised product, splitting it into sets of terms corresponding to valence-valence, valence-sea, sea-sea, etc., and then applying the appropriate phase space factor to each set of terms. Note that the phase space factor is no longer universal, but is nearly so – it turns out that this prescription is guaranteed to produce positive human basis dPDFs provided all the valence sPDFs are positive, which is the case for the set we have chosen.

With the choice (3.9), the dPDFs involved in number sum rules but which are not affected by number effects satisfy their sum rules to a much better degree. It also turns out that once we have included terms to take account of number effects (described shortly), insertion of phase space factors according to (3.9) into dPDFs affected by these effects similarly improves the degree to which these dPDFs satisfy the sum rules. What is more, the momentum sum rules are much better satisfied when one uses (3.9) rather than (3.7). Illustration of some of these points for some representative dPDF cases, as well as an exposition of the extent to which we satisfy the sum rules with this choice of phase space factor, is given in Fig. 5.

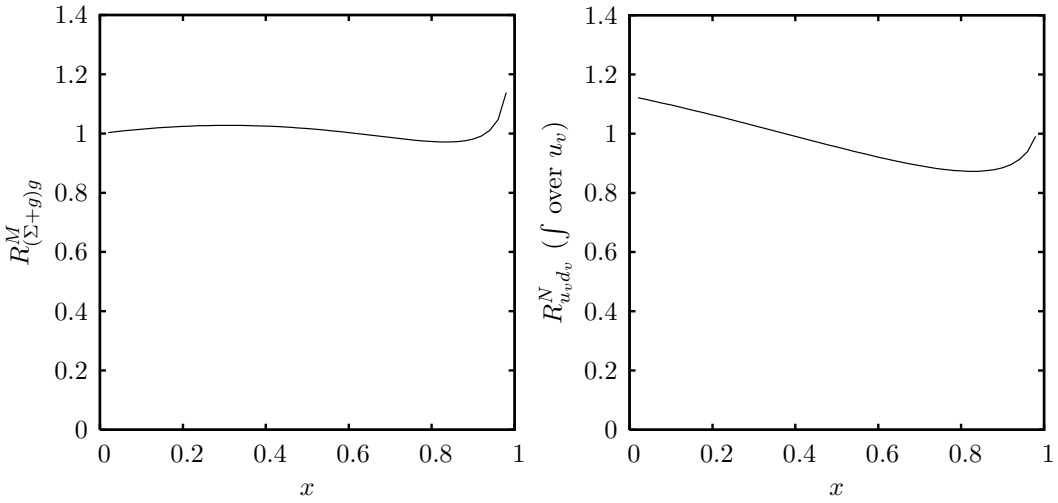

Figure 5: The same sum rule ratios as in Fig. 4, but this time plotted with the phase space factor as in (3.9).

Having found a satisfactory phase space factor, we proceed to discuss how the second required feature in the list above – namely the incorporation of number effects – might be achieved in our input dPDFs. We have seen that number effects are particularly important for equal flavour valence-valence dPDFs, and we shall outline how suitable inputs for this particular type of dPDF may be constructed shortly. However, number effects can also in principle have an impact on any other dPDF for which the same parton type appears in both parton indices. Since there are only a finite number of valence up and down quarks in the proton (as opposed to an infinite number of sea quarks and gluons), one might anticipate number effects relating to these valence quarks to be most important. We now discuss how these effects can be included in dPDFs which 'contain' an up and/or a down valence combination in both of their parton indices (e.g. u_+u_v, d_+d_+, where $i_+ \equiv i + \overline{i}$).

An example of such a distribution would be the u_+u_+ distribution, since $u_+u_+ = (u_v + 2u_s)(u_v + 2u_s)$, where $u_s = \overline{u}$. Consider the ways in which one can pick two up flavour partons (either quarks or antiquarks) from the proton. Either one can pick two sea partons, or one can pick a sea parton and a valence quark (in either order), or one can pick two valence quarks – these possibilities of course correspond to the different terms in the expansion of $(u_v + 2u_s)(u_v + 2u_s)$. Factorised terms multiplied by phase space factors are reasonable for all possibilities apart from the two valence option, where it would seem important to take account of the fact that removing a valence up halves the probability to find another. At a crude level we can incorporate this fact by using a term which is equal to half of the naive 'factorised $\times$ phase space factor' guess for the valence-valence term. We can think of this adjustment in another way, and say that we incorporate number effects in the u_+u_+ distribution by subtracting the following term from our initial 'factorised $\times$ phase space factor' construct:

$$\frac{1}{2} D_h^{u_v}(x_1;t_0) D_h^{u_v}(x_2;t_0) \rho^{u_v u_v}(x_1,x_2) \tag{3.11}$$

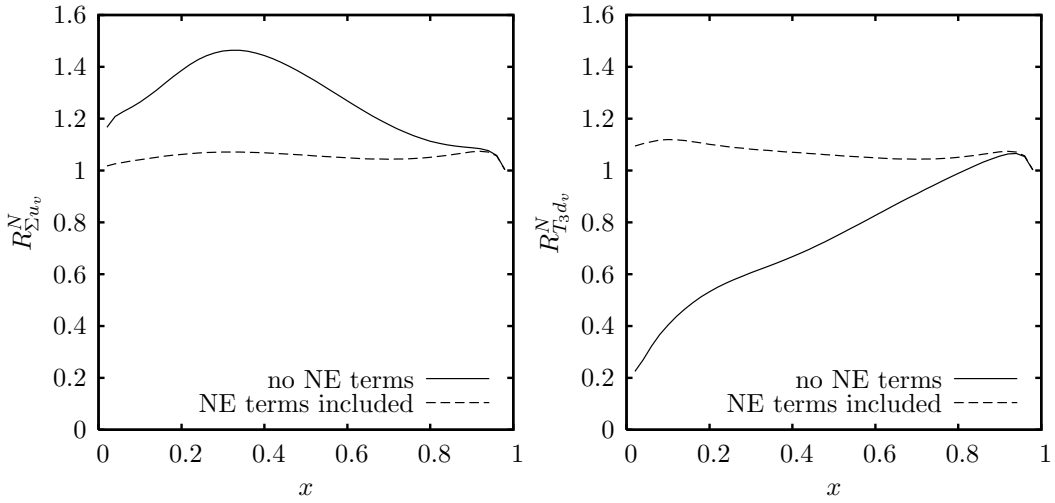

Figure 6: The effect of adding number effect (NE) terms on the sum rule ratios for the $u_v\Sigma$ and d_vT_3 number sum rules.

Generalising this argument, we observe that a dPDF which contains n times the up valence–up valence combination in its parton indices must have n times the term (3.11) subtracted from it to take account of number effects. Similarly, a distribution which contains n times the down valence-down valence combination in its parton indices must have n times $D_h^{d_v}(x_1;t_0)D_h^{d_v}(x_2;t_0)\rho^{d_vd_v}(x_1,x_2)$ subtracted from it. Note in this case that we must remove the naive d_vd_v term entirely because there is no chance of finding two valence down quarks in the proton. Fig. 6 shows how inclusion of the number effect terms improves the extent to which dPDFs satisfy number sum rules, for a few sample cases.

We now turn our attention to the construction of some equal flavour valence-valence dPDFs approximately satisfying the sum rules. The flavours we must be concerned about here are up, down, *and strange*. Note that the s_vs_v distribution is not zero with the given set of input sPDFs, even though the s_v sPDF is zero. The sum rule for this dPDF reads:

$$\int_0^{1-x_2} dx_1 D_h^{s_vs_v}(x_1,x_2;t_0) = -D_h^{s_+}(x_2;t_0) \tag{3.12}$$

Since the MSTW 2008LO s_+ input is nonzero, the right hand side of (3.12) is nonzero, and consequently the s_vs_v dPDF cannot be zero. We can explain why the s_vs_v distribution should be nonzero by expanding the combination into double human basis pairs – $s_vs_v = ss - s\bar{s} - \bar{s}s + \bar{s}\bar{s}$. We expect the probability to find an $s\bar{s}$ pair to be higher than that to find an ss or $\bar{s}\bar{s}$ pair due to number effects. Given that one has found a strange (antistrange) in the proton, the probability to find a further strange (antistrange) is reduced, whilst that to find an antistrange (strange) in addition remains the same.

In order to construct satisfactory distributions for these three flavour types, we imagine that there exists a scale $\tilde{t} < t_0$ at which only the three valence quarks in the proton may be resolved, and all sea distributions are zero. The sea distributions at t_0 are then generated dynamically by DGLAP evolution between $\tilde{t}$ and t_0. This idea has previously been put forward in [45–49], in which it was investigated whether the possibility exists to fit deep

inelastic scattering data using only u_v and d_v inputs at a fitted low scale $\tilde{t}$. As it turns out, one cannot achieve a fully satisfactory fit of data using this approach, as is admitted in [50]. However, since we shall only use this idea very loosely in what follows, this point is not of great concern to us.

At the scale $\tilde{t}$, the only equal flavour valence-valence dPDF which can be nonzero is the $u_v u_v$ distribution, as there is no possibility of finding two down or strange partons (be they quarks or antiquarks) at this scale. A suitable ansatz for the $u_v u_v$ at $\tilde{t}$ is a product of u_v sPDFs multiplied by a phase space factor $\tilde{\rho}$ appropriate at the scale, and divided by two to take account of valence-valence number effects:

$$D_h^{u_v u_v}(x_1, x_2; \tilde{t}) = \frac{1}{2} D_h^{u_v}(x_1; \tilde{t}) D_h^{u_v}(x_2; \tilde{t}) \tilde{\rho}^{u_v u_v}(x_1, x_2) \tag{3.13}$$

One can straightforwardly verify that the above forms for the equal flavour valence-valence dPDFs are consistent with the number sum rules at this scale. Now let us consider how the dPDFs change as we evolve from $\tilde{t}$ to t_0 under (2.1). The first two sets of terms on the RHS of (2.1) will mainly serve to take (3.13) into its equivalent at t_0 (and leave the other equal flavour valence-valence distributions zero). However, the final set of 'sPDF feed' terms results in an extra contribution appearing in each equal flavour valence-valence dPDF. Only the $-j\bar{j} - \bar{j}j$ component of an equal flavour valence-valence combination receives nonzero sPDF feed contributions during evolution ($g \to j\bar{j}$ contributions). Therefore, the sPDF feed for an equal flavour valence-valence dPDF is the following:

$$-2\frac{\alpha_s(t)}{2\pi} D_h^g(x_1 + x_2; t) \frac{1}{x_1 + x_2} P_{qg}\left(\frac{x_1}{x_1 + x_2}\right) \tag{3.14}$$

The splitting function P_{qg} is not a very strong function of its argument (only varying between $\frac{1}{2}$ and $\frac{1}{4}$). This means that, roughly speaking, we can take the sPDF feed term for the equal flavour valence-valence distributions as being a function of $(x_1 + x_2)$. If we then ignore the subsequent effect of the first two sets of terms on the RHS of (2.1) on the sPDF feed contributions, then we expect the sum total sPDF feed contribution to each valence-valence dPDF at t_0 to be a function of $(x_1 + x_2)$ only:

$$D_h^{j_v j_v}(x_1, x_2; t_0) = \frac{N_{j_v} - 1}{N_{j_v}} D_h^{j_v}(x_1; t_0) D_h^{j_v}(x_2; t_0) \rho^{j_v j_v}(x_1, x_2) - 2g^{j\bar{j}}(x_1 + x_2; t_0) \tag{3.15}$$

We shall refer to the function $g^{j\bar{j}}(x_1 + x_2; t_0)$ as the $j\bar{j}$ correlation term, as it represents the 'nonfactorised' part of the $j\bar{j}$ (or $\bar{j}j$) distribution which is built up from correlation-inducing sPDF feed contributions. How should we decide on the form of this function for a particular choice for the flavour j? We can answer this question by using the number sum rule that (3.15) must satisfy, which we shall write here as:

$$\int_0^{1-x_2} dx_1 D_h^{j_v j_v}(x_1, x_2; t_0) = (N_{j_v} - 1) D_h^{j_v}(x_2; t_0) - 2D_h^{\bar{j}}(x_2; t_0) \tag{3.16}$$

The first term on the RHS of (3.15) integrates to give approximately the first term on the RHS of (3.16). The $-2g^{j\bar{j}}(x_1 + x_2; t_0)$ must therefore integrate to give the second term

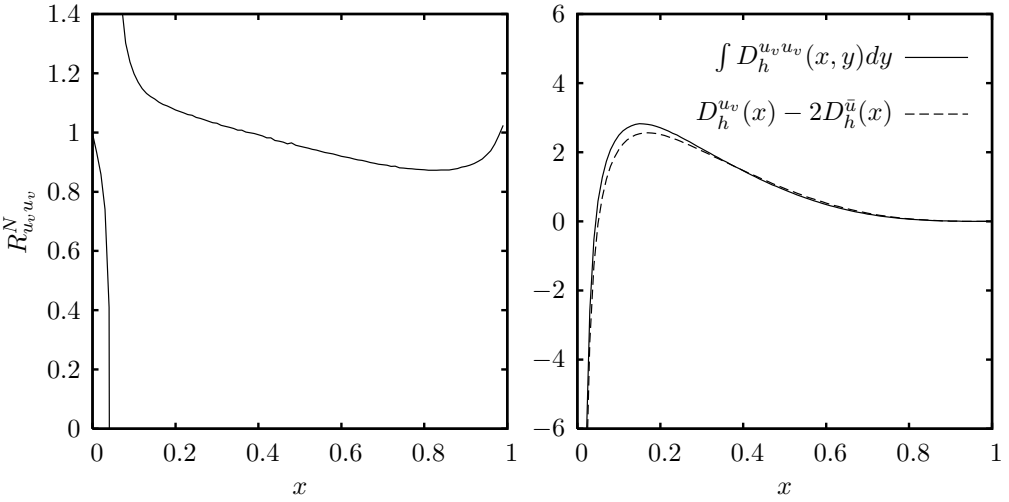

Figure 7: *Left panel*: The sum rule ratio for the $u_v u_v$ number sum rule when $D_h^{u_v u_v}$ is constructed according to (3.15) and (3.18). The ratio is close to 1 over most of the range of x, except near $x = 0.05$ where it diverges violently. This appears to indicate that the sum rule is being badly violated near $x = 0.05$.
Right panel: The $u_v u_v$ sum rule integral plotted against the sPDF quantity it should be equal to. This plot reveals that the divergence in the sum rule ratio is caused by the integral curve slightly missing a zero in the sPDF quantity, and is not serious in practice.

on the RHS of this equation:

$$-2\int_0^{1-x_2} dx_1 g^{j\bar{j}}(x_1 + x_2; t_0) = -2D_h^{\bar{j}}(x_2; t_0) \tag{3.17}$$

This is an integral equation with a unique solution, and it is straightforward to show that the solution is the following:

$$g^{j\bar{j}}(x; t_0) = -\frac{\partial D_h^{\bar{j}}(x; t_0)}{\partial x} \tag{3.18}$$

Our proposed form for the input equal flavour valence-valence distributions is therefore (3.15) with $g^{j_v j_v}$ given by (3.18). Clearly the $d_v d_v$ and $s_v s_v$ number sum rules will be perfectly satisfied using this form. Fig. 7 shows how well the $u_v u_v$ sum rule is satisfied.

Unfortunately, with this choice for the equal flavour valence-valence dPDFs, the $\bar{u}\bar{u}$, $\bar{d}\bar{d}$, ss and $\bar{s}\bar{s}$ dPDFs all go negative. Naively, one might view this as arising because the forms we have used for the equal flavour valence-valence dPDFs are in some way unsatisfactory. However, instead we observe that it occurs because we have omitted an important term in our above treatment of the $j_+ j_+$ distributions. Since these distributions contain the parton combination $j\bar{j} + \bar{j}j$ that also appears in the $j_v j_v$ distribution with the opposite sign, the $j_+ j_+$ receive the same sPDF feed contributions as the $j_v j_v$ during evolution, but with the opposite sign. Thus for consistency each $j_+ j_+$ distribution should have an extra term added onto it equal to *plus* $2g^{j\bar{j}}(x_1 + x_2; t_0)$. With this alteration, all double human

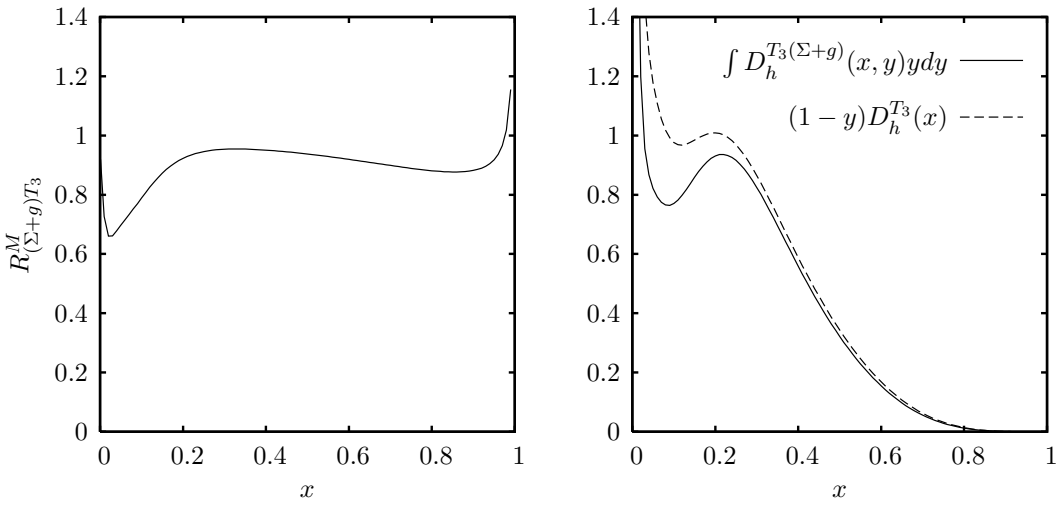

Figure 8: *Left panel*: The sum rule ratio for the $(\Sigma + g)T_3$ momentum sum rule, plotted using the fully constructed set of input dPDFs.
Right panel: The $(\Sigma+g)T_3$ momentum sum rule integral plotted against the sPDF quantity it should be equal to.

basis dPDFs are again positive, and we see little adverse effect on the extent to which the sum rules involving j_+j_+ distributions are satisfied.

Having now completed our description of how we constructed some suitable input dPDFs, we conclude our discussion with a short summary of how well the dPDFs satisfy the complete set of sum rules. In the context of the double human basis, the sum rule ratios are all within 25% of 1 for $x \lesssim 0.8$. Above this value, the sum rules are not obeyed so well – however the values of the PDFs are tiny at these x values, so large/small sum rule ratio values at these x values are not in practice too great a problem. In the double evolution basis the story is the same, barring trivial divergences due to the sum rule integral slightly missing a zero in the sPDF quantity it should be equal to. The one exception to this is the case of the $T_3(\Sigma + g)$ momentum sum rule. The sum rule ratio for this sum rule, plotted in the left panel of Fig. 8, plunges to 0.65 around $x = 0.02$. This possibly looks worse than it is – if one plots both the integral and the sPDF quantity it should be equal to (right panel of Fig. 8), then one notices that the dip in the sum rule ratio is due to the integral slightly overestimating a dip in the sPDF quantity in a region where the sPDF quantity is rather small. Furthermore, it is unlikely that the particular combination $T_3(\Sigma + g)$ will be directly accessed by any scattering processes at the LHC. Consequently we are prepared to accept the large deviation from 1 in the $T_3(\Sigma + g)$ sum rule ratio.

4. Numerical Solution of the Double DGLAP Equation

There exist several options for the broad numerical method to use to integrate the dDGLAP equations. One could choose to adapt either the direct x space or Mellin transform methods which are commonly used to numerically integrate the sDGLAP equation (see, for example, [51,52] for routines using the x space method for solution of the sDGLAP equation, and [53]

for a routine using the Mellin transform method). Alternatively, one could develop a numerical method based on the explicit solution of the dDGLAP equation in terms of sPDFs (2.8). This is the approach that has been preferred in the previous numerical treatments of the subject [37, 38]. Here we adopt an x space method. This has the advantages that it is conceptually simple, is flexible enough to take the inputs described in Section 3.2 with no problems, and is competitive in efficiency with the other methods in the context of the dDGLAP equation. It also has the advantage over the 'explicit solution' method in that the $D_i^j(x;t)$ Green's functions, which are difficult to calculate numerically to a sufficient degree of accuracy, do not feature.

4.1 The dDGLAP Evolution Program

Our program solves the dDGLAP equation (2.1) directly using a grid in x_1, x_2 and t. We choose the spacing of the grid points in t to be linear – this is the 'natural' choice, and it is adopted in a number of sDGLAP x-space routines (e.g. [51,52]). In the x_1 and x_2 directions, the points are taken to be evenly spaced in the variable $u = \ln(\frac{x}{1-x})$, with equal numbers of points in the x_1 and x_2 directions (600 for the grids of [40]). This gives a spacing uniform in $\ln(x)$ in the small x regions and directions in which the dPDF is diverging rapidly, and a linear spacing in larger x regions and directions in which the variation of the dPDF is slower. The boundary of the grid in (x_1,x_2) space is defined by the lines $x_1 = x_{\min}$, $x_2 = x_{\min}$, $x_1 = 1 - x_{\min}$, $x_2 = 1 - x_{\min}$, and $x_1 + x_2 = 1$ (the kinematical boundary), with a default $x_{\min} = 10^{-6}$. The methods we use for the numerical integration of the first two terms on the right hand side of the dDGLAP equations are described in the Appendix.

The final set of terms in the dDGLAP equation (the 'sPDF feed' terms) are obtained at a given t by numerically evolving the sDGLAP equations contemporaneously with the dDGLAP equations. The grid used for the sDGLAP evolution is the similar to that used for the dDGLAP evolution. The only difference is that it extends in just one x direction, between $x_{\min}$ and $(1-x_{\min})$. For consistency, the sPDF inputs used are the MSTW2008LO inputs.

Given the structure of the dDGLAP equation, the dDGLAP evolution routine requires the values of the sPDFs at x values of the form $x_i + x_j$, where x_i and x_j are two x values on the uniform in $\ln(x/(1-x))$ grid. With the grid used, it is clear that $x_i + x_j$ does not also lie on the grid, so interpolation has to be used to obtain the sPDF values required. Away from the edges of the sPDF x-grid, natural cubic spline interpolation based on the sPDF values at the nearest four grid points is used, whilst linear interpolation is used at the edges.

The program uses the 'double evolution' basis introduced in Section 3 as its internal basis for the evolution of the dPDFs. Use of this basis for the evolution is advantageous because the dDGLAP equations become in some sense 'minimally coupled' in this basis. Out of the 91 equations, 66 are rendered diagonal at LO using this basis (i.e. rate of change of D_h^{ij} with t is given only by the two integral terms involving D_h^{ij}, with no nonzero sPDF feed terms). The remaining equations have very few terms on the RHS (two terms in each integral term plus one sPDF feed term). The use of this basis makes the coding in of the dDGLAP equations manageable.

Stepwise evolution in t is carried out by a fourth-order Runge-Kutta method. The evolution begins at a scale t_0 equal to that at which the input distributions are defined ($Q_0^2 = 1$ GeV^2 with the MSTW2008LO inputs). The final scale obtained in the evolution t_f and the number of Runge-Kutta steps used to reach this scale N_t may be specified by the user. To produce the grids of [40], 120 points were used in the t direction.

4.2 Flavour Number Schemes

Our program has the potential to perform the evolution using either a fixed or (zero mass) variable flavour number scheme, with n_f fixed at $3, 4, 5$ or 6 in the FFNS, or potentially varying from $3 \to 6$ in the ZM-VFNS. The scheme can be determined by the user via the variables `LGMCSQ`, `LGMBSQ` and `LGMTSQ` which are equal to the thresholds in t at which the charm, bottom and top flavours become active respectively. For a FFNS of given n_f, `LGMCSQ`, `LGMBSQ` and `LGMTSQ` should be set appropriately either above t_0 or below t_f (e.g. for a FFNS with $n_f = 5$, set `LGMCSQ` $< t_0$,`LGMBSQ` $< t_0$ and `LGMTSQ` $> t_f$). For a ZM-VFNS, at least one of `LGMCSQ`, `LGMBSQ` and `LGMTSQ` must lie in between t_0 and t_f. It should be noted that to produce the grids of [40], the program was run under a ZM-VFNS with n_f varying between 3 and 5. The variables `LGMCSQ` and `LGMBSQ` were set according to the values of m_c and m_b preferred by MSTW – 1.40 GeV and 4.75 GeV respectively.

Prior to the evolution, the program compares `LGMCSQ`, `LGMBSQ` and `LGMTSQ` with t_0 and t_f. Depending on the results of this, it splits the full evolution from t_0 and t_f into up to four intervals, each with a different value of n_f. The total number of integration steps in t, N_t, is divided up amongst these intervals roughly in proportion to the interval sizes in t.

In each interval, the strong coupling constant t is calculated according to the LO analytic form:

$$\alpha_S(t) = \frac{\alpha_S(t')}{1 + \alpha_S(t')b(t - t')}; \quad b \equiv \frac{33 - 2n_f}{12\pi}. \tag{4.1}$$

The quantity t' corresponds to the value of t at the beginning of the interval. In the first interval, the boundary value of the strong coupling constant, $\alpha_S(t')$, is taken to be the initial value specified by the user $\alpha_S(t_0)$. In later intervals it is chosen to ensure continuity in α_S, which is the appropriate matching condition at LO [41].

4.3 Accuracy of the Program

We wish to get a rough estimate of the error in the dPDF values at Q introduced by numerical evolution with N_x points in each x direction, and N_t points in the t. To do this, one might propose doing an evolution with twice as many points in each direction, and then taking the error in the original dPDFs at Q as being the absolute difference between the dPDF values produced by the two evolutions. Unfortunately, we cannot perform this procedure for the values of N_x and N_t used to produce the grids in [40] (600 and 120). This is because doubling the number of x points in this case causes the program to require far more RAM than a typical modern machine can provide. Instead, we show here that the accuracy of the program is reasonable even when N_x and N_t take on the smaller values of

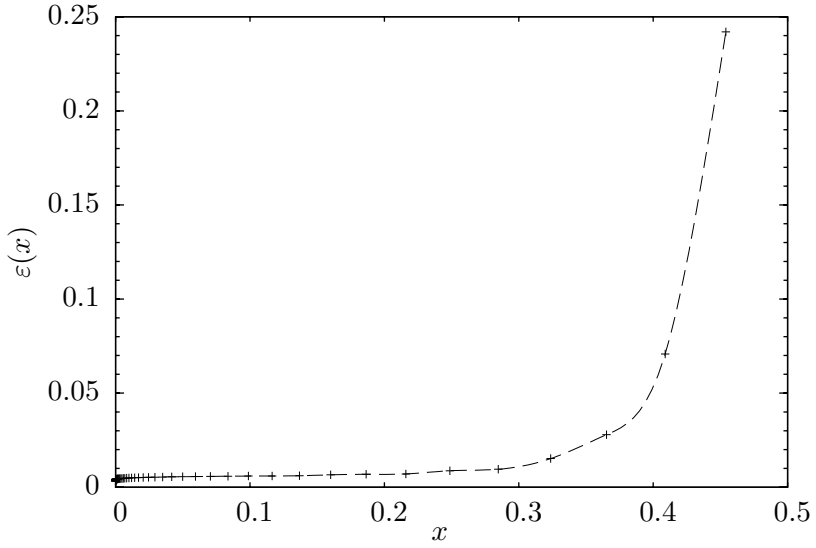

Figure 9: An estimation of the numerical error when one performs an evolution from $Q = 1$ GeV to $Q = 100$ GeV using a grid with 150 points in each x direction, and 10 in the t. The error values plotted are those in the gg dPDF along the line $x_1 = x_2 = x$.

150 and 10 respectively – we then know that the accuracy of the procedure with $N_x = 600$ and $N_t = 120$ should be very good.

We perform the error estimation evolution from $Q_0 = 1$ GeV to $Q_f = 100$ GeV. In Fig. 9, the fractional error in the distribution D_h^{gg} along the sample line $x_1 = x_2 = x$ as calculated by the above method is plotted. That is, we plot:

$$\varepsilon(x; Q_f) \equiv \frac{\mid D_h^{gg}(x, x, Q_f)_{N_x=150, N_t=10} - D_h^{gg}(x, x, Q_f)_{N_x=300, N_t=20} \mid}{D_h^{gg}(x, x, Q_f)_{N_x=300, N_t=20}}. \tag{4.2}$$

We choose to look at D_h^{gg} because this is one of the dPDFs which should be calculated least accurately by an evolution routine. As expected, the error increases as one approaches the kinematical bound due to the fact that less x points are used in the evolution integrations for the dPDF values closer to the bound. We see that the error is small in the crucial small x region – less than 1% for $x \lesssim 0.3$, and less than 6% for $x \lesssim 0.4$. The error becomes large as one approaches $x = 0.5$, but since this region is not likely to be important in applications at the LHC (which probes $x_1, x_2 \lesssim 0.1$), this is not a major problem. The graph indicates that even with $N_x = 150$ and $N_t = 10$ the numerical evolution to LHC scales introduces errors which are less than 1% for $x_1 < 0.3, x_2 < 0.3$, and less than 6% for $x_1 < 0.4, x_2 < 0.4$.

5. Properties of the dPDFs

We have seen that there are two ways to improve on using simple products of sPDFs as the dPDFs at the (high) scale Q. First, one can use dDGLAP evolution to obtain the dPDFs at Q, with a reasonable choice of dPDFs at a low scale Q_0 used as the starting point for the

evolution. Second, one can use improved inputs at the low scale Q_0, which take account of momentum and number effects. In this section, we describe and illustrate the extent to which introducing these improvements changes the dPDFs at the scale Q.

The large number of dPDFs precludes the possibility of discussing them all. Instead, we choose to focus on a small number of parton pairings which should be important in double scattering processes at the LHC, and which in some sense might be considered to form a representative set. These are the uu, $u\bar{u}$, ug and gg pairings. Note that we have a dPDF for which our input form contains a valence number effect term in this set (the uu), and a distribution for which our input contains a $j\bar{j}$ correlation term (the $u\bar{u}$). Furthermore, we see that the set covers all types of sPDF feed term that can appear in dDGLAP evolution.

For the purposes of making concrete comparisons between different methods of obtaining the dPDFs at a high scale Q, we also need to make a specific choice for Q. Except where otherwise stated, we make the reasonable choice $Q = 100$ GeV ($\sim M_W, M_Z$, for example). At the scale Q, we only look at the dPDF values along the line $x_1 = x_2$ – this allows us to produce easily readable 2D plots.

The main novel component of the present work is the introduction of the improved input dPDFs of Section 3.2. Consequently, the first question we should like to answer is how use of the improved inputs in the dDGLAP equation, as opposed to naive 'factorised$\times(1-x_1-x_2)^p$' inputs, affects the dPDFs at the scale Q. To this end, we have plotted the following ratio for our sample dPDFs in Fig. 10:

$$R^{ij}_{\Delta input}(x;Q) \equiv \frac{D^{ij}_h(x,x;Q)\mid_{\text{input } D^{ij}_h(x_1,x_2;Q_0)=D^i_h(x_1;Q_0)D^j_h(x_2;Q_0)(1-x_1-x_2)^p}}{D^{ij}_h(x,x;Q)\mid_{\text{input } D^{ij}_h(x_1,x_2;Q_0)=\text{our improved inputs}}} \tag{5.1}$$

We have made plots for each of the common traditional choices for p – 0, 1 and 2. One immediately notices in Fig. 10 that all of the ratio curves deviate significantly from 1. This shows that the precise choice of inputs at the low scale has an important impact on the high scale dPDFs, and demonstrates the inadequacy of the traditional naive input forms. We see that multiplying factorised inputs by a phase space factor of $(1-x_1-x_2)$ or $(1-x_1-x_2)^2$ gives high scale dPDFs which are generally too small for small (x_1, x_2). This is expected – we have seen that $(1-x_1-x_2)$ or $(1-x_1-x_2)^2$ phase space factors suppress the inputs too much in the high x_1, low x_2 and high x_2, low x_1 regions. Since these regions directly feed the small x_1, x_2 region, this directly translates into a deficiency in the high scale dPDFs in the small x_1, x_2 region. Conversely, we see that not using a phase factor in the inputs results in high scale dPDFs which are generally too large. This is because in this scenario the inputs are too large near the kinematic bound, and this excess propagates down to smaller x_1, x_2 values during evolution.

It is interesting to note that, contrary to the previous general statement, the $p = 0$ ratio for the $u\bar{u}$ dPDF actually dips below unity between $x = 0.005$ and $x = 0.15$. Furthermore, we see that the $p = 0$ uu ratio rises above the corresponding ratios for the other flavour combinations. The origin of each of these features is in the extra terms we included in our improved inputs to take account of valence number effects or $j\bar{j}$ correlations, which

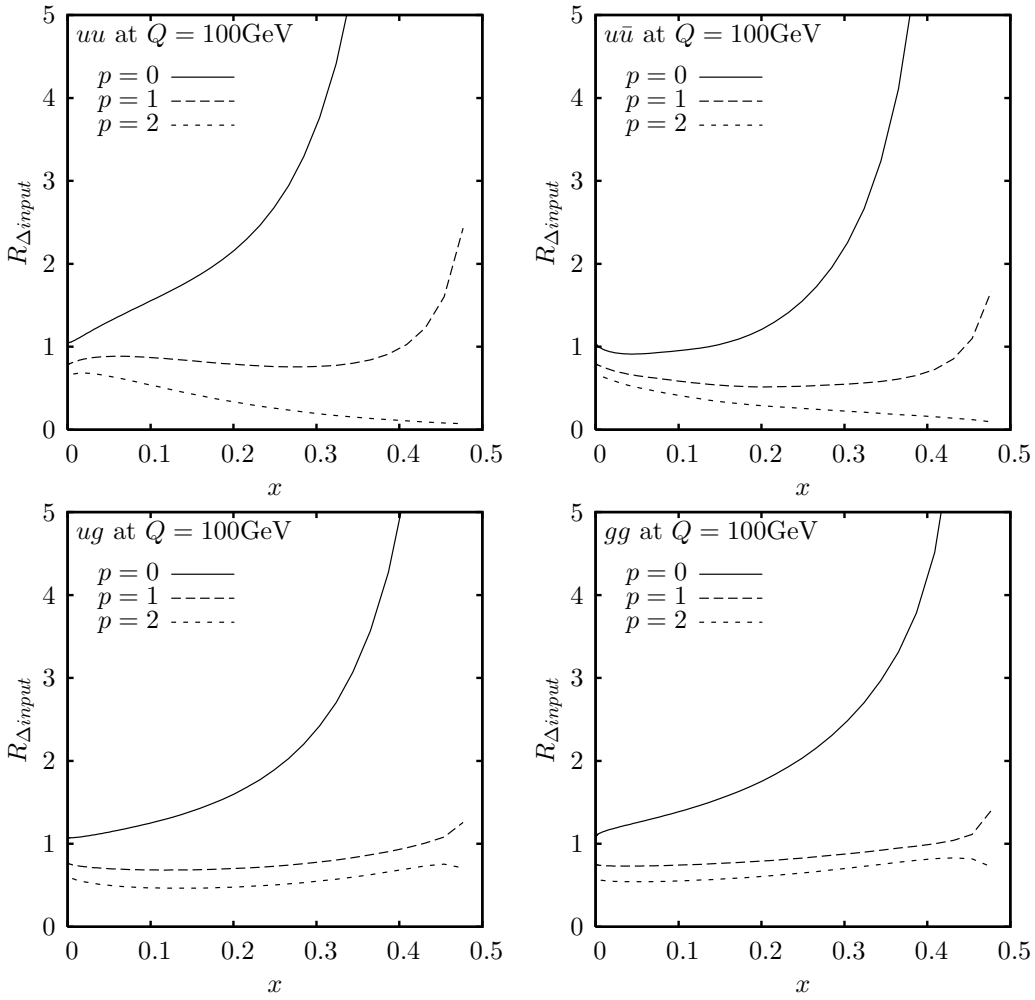

Figure 10: Plots of the ratio $R^{ij}_{\Delta input}$ defined in equation (5.1) for $Q = 100$ GeV, $p = 0, 1$ and 2, and the parton combinations ij discussed in the text.

do not appear in the naive inputs. The inclusion of a positive $j\bar{j}$ correlation term in the $u\bar{u}$ distribution causes our $u\bar{u}$ dPDF to be larger at the high scale than it would be if the correlation term were absent. Since our dPDFs appear on the denominator of $R^{ij}_{\Delta input}$, this manifests itself as a reduction in our $p = 0$ $u\bar{u}$ ratio. Conversely, the subtraction of a valence number effect term from our uu input results in a reduction of our uu dPDF at Q, which increases the uu ratio.

For $p = 1$ and 2, we observe that the uu ratio is still larger than the others for small x. However, the $u\bar{u}$ ratio is now very slightly larger than the ug and gg ratios at small x values. This is because the ug and gg high scale distributions at small x are more sensitive to the form of the input distributions near the kinematic boundary than the $u\bar{u}$. This is a simple consequence of the fact that gluon type evolution causes a faster cascade of PDFs to low x values than u or $\bar{u}$ type evolution. The reduction in the ug and gg ratios at small x relative to the $u\bar{u}$ due to the change in p overcomes the small effect of including the $j\bar{j}$ correlation term in our $u\bar{u}$.

The contributions of the $j\bar{j}$ correlation and valence number effect terms to the high scale ($Q = 100$ GeV) double human basis dPDFs are most cleanly observed at $x \sim 0.05$, and are on the order of 10% in this x region. For smaller x, the contributions from the extra terms are swamped by sea-sea contributions to the dPDF, whilst at larger x, phase space effects become dominant.

Aside from looking at the effect of using different inputs on the dPDFs at scale Q, we can also ask to what extent correlations introduced by dDGLAP evolution affect the dPDFs at Q. There are essentially two types of correlations that the dDGLAP equation introduces – correlations due to the requirement of momentum conservation, and more interesting correlations generated by the sPDF feed terms. Here, we choose to look specifically at the effect of the latter.

In order to do this, we evolved our improved input dPDFs up to the scales $Q = 10$ GeV, $Q = 100$ GeV, and $Q = 1000$ GeV, both with the sPDF feed terms included in the evolution, and also with these terms set to zero. For each final scale and parton pairing in our selected set, the following ratio was then plotted:

$$R^{ij}_{\text{no feed}}(x;Q) \equiv \frac{D^{ij}_h(x,x;Q)\mid_{\text{our improved inputs, no sPDF feed}}}{D^{ij}_h(x,x;Q)\mid_{\text{our improved inputs}}} \tag{5.2}$$

The results are given in Fig. 11. The effect of the sPDF terms is small but non-negligible, being at roughly the 10% level for $x < 10^{-2}$ in all of the dPDFs considered, and increasing with Q.

We observe that the ratios for all of the given flavour combinations look very similar for x from 10^{-6} to 10^{-4}. The reason for this is that the small x shape of the distributions considered is very strongly determined by the (either direct or indirect) feeding of these distributions by the gg distribution. If the gg dPDF loses its sPDF feed and is reduced by a certain percentage at small x, the connection of the other dPDFs to the gg will result in these dPDFs being reduced by a similar amount. This explanation can be verified by investigating what happens if we remove all of the sPDF terms except for the gg feed. In this case the ratios for all of the considered dPDFs are much closer to 1 for $10^{-6} < x < 10^{-4}$, suggesting that the subtraction of the gg sPDF feed is the dominant factor determining the shapes of the plots in Fig. 11 for small x.

For larger x, the deviation of the uu ratio from 1 remains small, and tends to 0 as x approaches its maximum of 0.5. This is expected since there is no direct sPDF feed term in the evolution of the uu dPDF. The $u\bar{u}$ ratio also seems to tend to 1 as $x \to 0.5$, albeit more slowly, whilst the ug and gg ratios plunge towards zero, the gg more rapidly than the ug. This implies that at large x, the sPDF feed contributions are more important to the gg than they are to the ug, and that they are more important to the ug than they are to the $u\bar{u}$. We can explain this ordering using a fact we have previously mentioned – namely, that the 'pull' on a gluon PDF towards lower x values during evolution is stronger than that on a quark type PDF. The gg distribution at large x is pulled strongly towards lower x values in two directions, and is very much smaller if it is not continuously fed by an sPDF. By contrast, the 'pull' on the large x $u\bar{u}$ distribution is smaller in both directions, and so the contribution of similar sPDF feed terms is proportionately smaller. The ug distribution

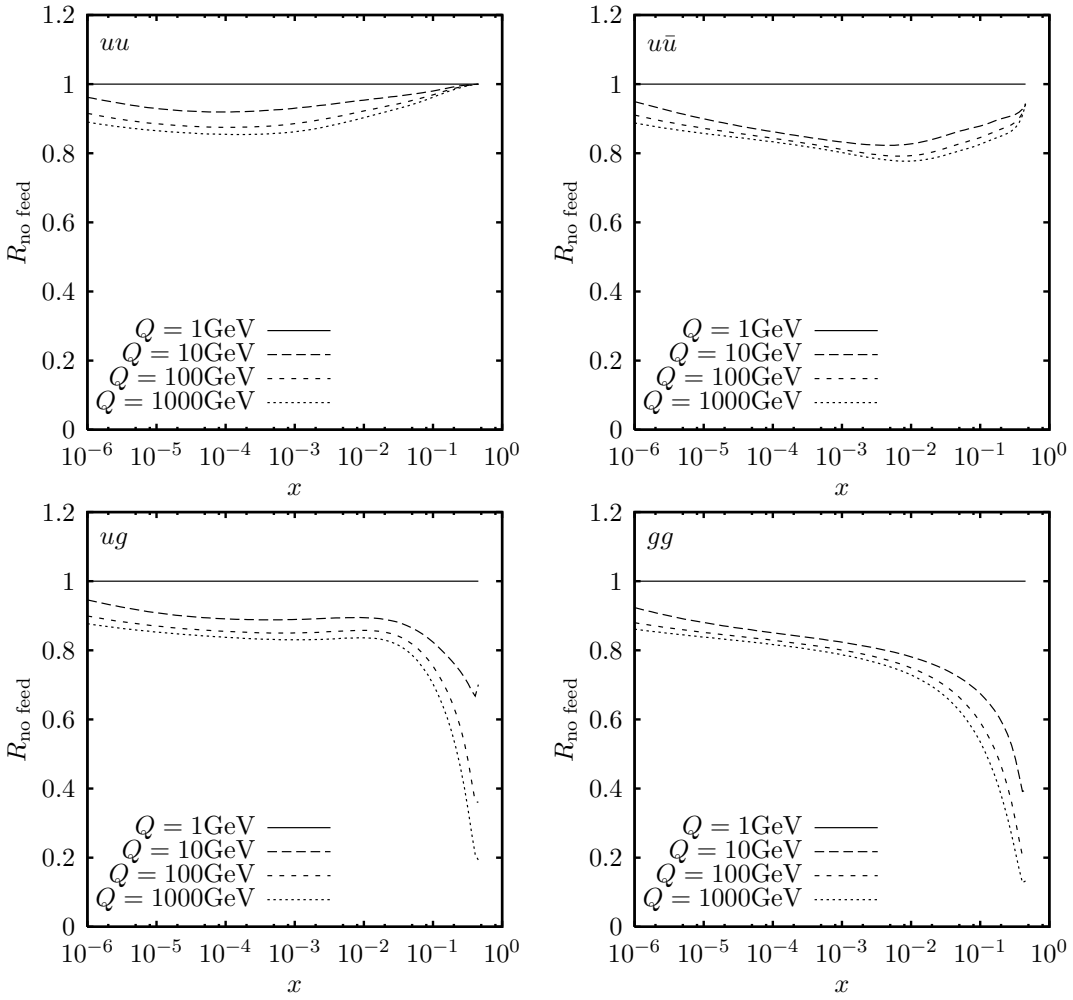

Figure 11: Plots of the ratio $R^{ij}_{\text{no feed}}$ defined in equation (5.2) for $Q = 1, 10, 100$ and 1000 GeV and the parton combinations ij discussed in the text.

has one gluon flavour index and one quark, so the importance of the sPDF feed on this distribution at large x is intermediate.

We have not been able to exactly reproduce the results of either of the extant numerical investigations into the correlations induced by evolution – [37] and [38]. However, we do agree with [38] that the accumulated sPDF feed contribution to the gg between ~ 1 GeV and 100 GeV accounts for about 10% of the $Q = 100$ GeV gg distribution at small x. In Fig. 12, we plot the following ratio for $Q = 80.4$ GeV:

$$R^{gg}(x;Q) \equiv \frac{D_h^{gg}(x,x;Q)\,|_{\text{factorised inputs}} - D_h^g(x;Q)D_h^g(x;Q)}{D_h^g(x;Q)D_h^g(x;Q)} \tag{5.3}$$

This figure corresponds to the solid curve in Fig. 1 of [37], with MSTW2008LO inputs replacing the MRS99 inputs used there. We expect that the ratio R^{gg} should tend to -1 as x approaches 0.5 for any Q sufficiently larger than the input scale. This is because evolution will very quickly cause D_h^{gg} to become much smaller than the factorised value

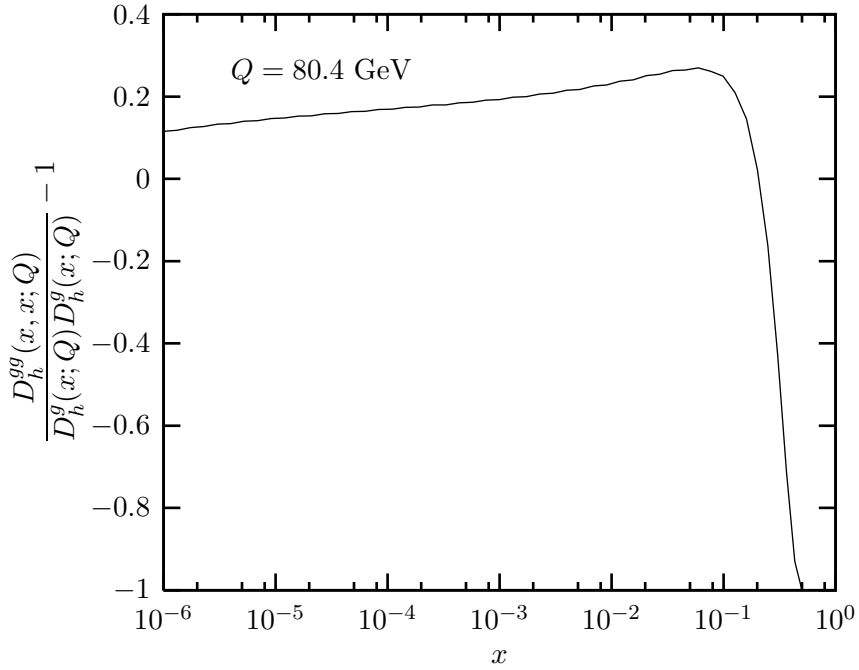

Figure 12: gg correlation ratio R^{gg} at $Q = 80.4$ GeV obtained using MSTW2008LO factorised inputs.

near the kinematic bound. Our curve exhibits this property, but it seems unlikely that the solid curve plotted in Fig. 1 of [37] will, especially if it reaches 0.6 for higher x values as is stated in [37].

Finally, we compare our full treatment (improved inputs plus full dDGLAP evolution) with the approximation that simply uses factorised inputs $\times(1-x_1-x_2)^p$ ($p = 0, 1$ or 2) at the scale Q. This approximation is frequently used in phenomenological studies of double parton scattering processes. In Fig. 13, we plot the following ratio along the line $x_1 = x_2 = x$ for our sample dPDFs and for $p = 0, 1$ and 2:

$$R^{ij}_{\Delta final}(x_1, x_2; Q) \equiv \frac{D_h^i(x_1;Q) D_h^j(x_2;Q)(1-x_1-x_2)^p}{D_h^{ij}(x_1, x_2; Q) \mid_{\text{our improved inputs}}} \tag{5.4}$$

The plots reveal that even a $(1-x_1-x_2)^2$ phase space factor multiplying a factorised form at Q underestimates the large x falloff in the dPDFs along $x_1 = x_2 = x$. For very small x, the ratios are all slightly less than 1 due to the fact that one misses the sPDF feed contributions if one uses a factorised form at Q (note that the ratio appears smallest at very low x for the $u\bar{u}$, due to the fact that the sPDF feed for the $u\bar{u}$ is particularly important around $x = 10^{-2}$ – see Fig. 11). One also notices the imprint of omitting the valence number effect and $j\bar{j}$ correlation terms in the ratios – the uu ratio rises above the others at $x \sim 0.05$, whilst the $u\bar{u}$ dips at this x value.

It is interesting to consider the behaviour of $R^{ij}_{\Delta final}(x_1, x_2; Q)$ away from the line $x_1 = x_2 = x$. In Fig. 14, we plot the $p = 0$ ratio for the gg flavour combination along several lines emanating from the point $x_1 = 10^{-6}, x_2 = 10^{-6}$. The figure shows that the

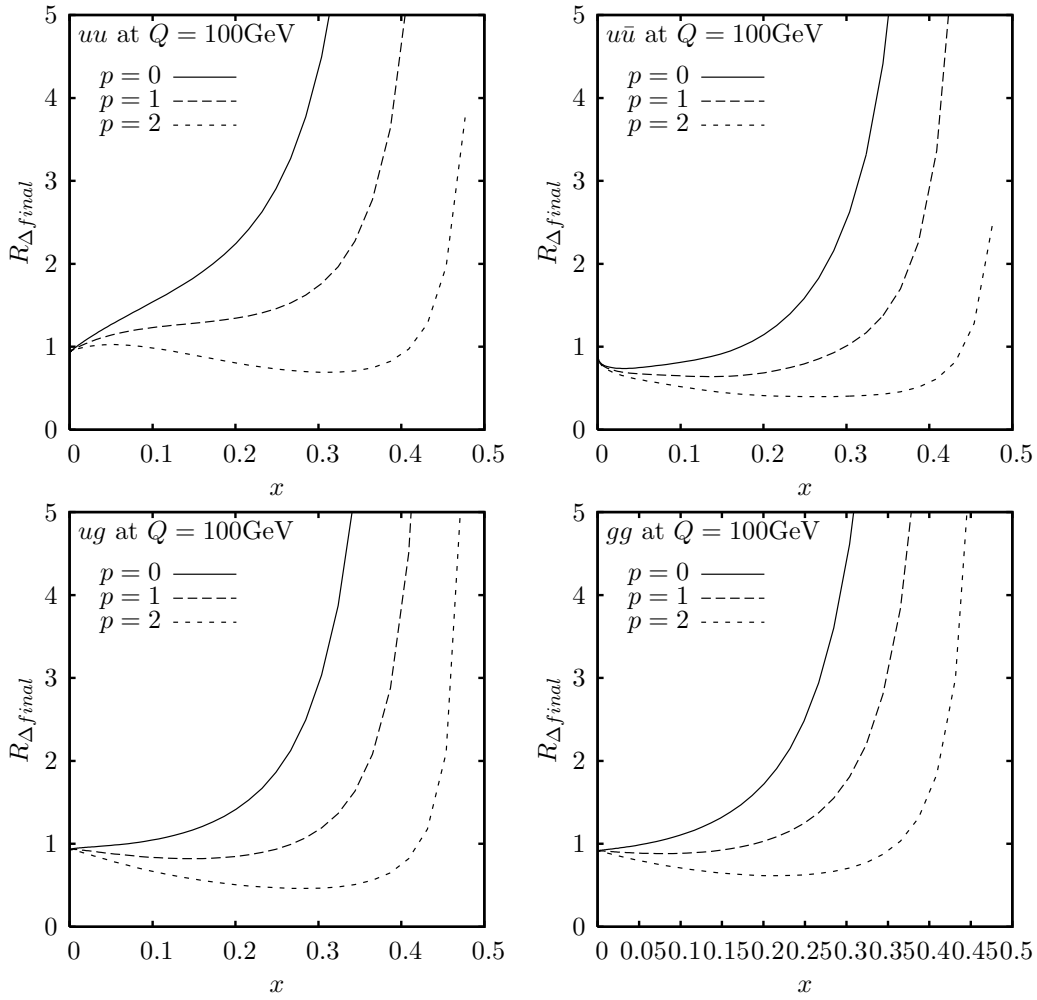

Figure 13: Plots of the ratio $R^{ij}_{\Delta final}$ defined in equation (5.4) at $Q = 100$ GeV and along the line $x_1 = x_2 = x$. The ratio is plotted for $p = 0, 1$ and 2 and for each of the parton combinations ij discussed in the text.

deviation of this ratio from 1 is maximal along $x_1 = x_2$ (in fact, this statement holds for any combination of parton indices). We observe that a $p = 0$ factorised form is a fairly good approximation to our gg dPDF close to the x_1 axis, except when x_1 is very large ($x_1 > 0.8$). This is to be expected, given our use of input dPDFs which essentially reduce to $p = 0$ factorised forms near the lines $x_1 = 0$ and $x_2 = 0$. One can infer from the plot that use of a factorised form multiplied by either $(1 - x_1 - x_2)$ or $(1 - x_1 - x_2)^2$ will result in one overestimating the falloff in the dPDFs in the $x_1 \sim 0, x_2 \lesssim 0.8$ and $x_1 \lesssim 0.8, x_2 \sim 0$ regions.

6. Summary and Outlook

In this report, we have developed a framework based on the dDGLAP equation for calculating the LO double distributions $D^{ij}_h(x_1, x_2; t)$ which represents an improvement on

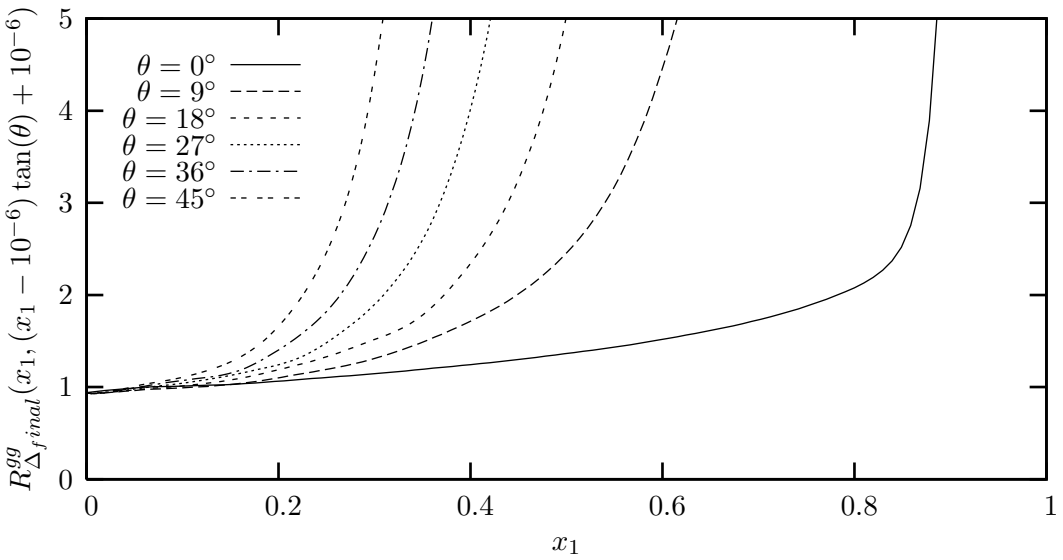

Figure 14: The ratio $R^{gg}_{\Delta final}$ plotted along various lines of the form $x_2 = (x_1 - 10^{-6})\tan(\theta) + 10^{-6}$ at $Q = 100$ GeV.

approaches used previously. We have derived for the first time the momentum and sum rules that the dPDFs have to obey. An important implication of these sum rules is that the conventionally held wisdom that the dPDFs should be approximately equal to products of sPDFs for small x_1, x_2 does not apply in the case of the equal flavour valence-valence dPDFs. Using the dPDF sum rules, we have constructed a set of improved input dPDFs corresponding to the MSTW2008LO sPDF inputs. In the double human flavour basis, these dPDFs are all positive and satisfy the sum rules to better than 25% precision.

We have written a program which numerically integrates the LO dDGLAP equation using a direct x space method, enabling one to evolve the dPDF inputs to higher scales. The accuracy of the program is good for small x_1, x_2 – an evolution from 1 GeV to 100 GeV using a grid with only 150 points in each x direction and 10 points in the t direction produces dPDF values with numerical errors of less than 1% for $x_1 < 0.3, x_2 < 0.3$. We have produced a set of publicly available dPDF grids by applying the numerical procedure to our improved inputs, which can be found along with interpolation code at [40]. To produce the grids, 600 points were used in each x direction, and 120 in the t, ensuring an accuracy much better than 1% for small x.

We saw that the accuracy of our program is rather poor near the kinematical bound. If the accuracy here needed to be improved without significantly increasing computing time, then a multigrid method could be implemented in the program (for an example of the use of this method for the sPDF case, see [51]). The additional more finely spaced grids would be introduced in the region near the kinematic bound to increase accuracy in this region.

For the purposes of experimental studies of double parton interactions in the near future, which will be attempting to establish the existence of correlations in the dPDFs, the LO treatment presented here is sufficiently accurate. If correlations are found and they agree with some or all of the predictions made here, then this will be a strong impetus for us

to extend the formalism to NLO. As mentioned in Section 2, such an extension is not trivial, since the structure of the third term of the dDGLAP equation becomes significantly more complex at NLO. At this order, one requires the functions $P^{(1)}_{i\to jk}(x_1, x_2)$ which cannot be obtained trivially from the NLO sPDFs as in the LO case. It is likely that these functions exist in the literature, although some work may need to be done to get them into a form that can be used in the dDGLAP equation.

Many double scattering processes which might provide important signals/backgrounds at the LHC do not involve the same hard scale in both collisions. An example of such a process is the simultaneous production of a W and a $b\bar{b}$ pair in separate collisions. This forms a background to the process $p + p \to WH$, $H \to b\bar{b}$, which might be an important process to discover the Higgs if $m_h < 2m_W$ [20]. To make theoretical predictions relating to these processes, we require the more general double distributions with $t_1 \neq t_2$. As is mentioned in Section 2, we believe that these distributions are calculated by adding an extra sDGLAP evolution in one variable on top of the dDGLAP evolution. A useful extension to the work would be to produce a more general set of double distributions based on this hypothesis.

Finally, there exists the possibility of using the dPDFs developed above to undertake a phenomenological investigation of double parton scattering at the LHC. In particular it would be interesting to examine how the 'correlations' introduced via our inputs and by evolution affect the properties of a double scattering event, and also how one might measure the correlations in practice. We are currently in the process of making such an investigation.

Acknowledgements

JG acknowledges financial support from the UK Science and Technology Facilities Council.

Appendix

A. Numerical techniques for evaluating the dDGLAP integrals

Let us consider the integrals which have to be numerically approximated using the (x_1, x_2) grid. All of these integrals are of the following schematic form:

$$I(y) = \int_x^{1-y} \frac{dz}{z} D(z,y) P\left(\frac{x}{z}\right) \tag{A.1}$$

The splitting function $P(x)$ may in general consist of three terms. The first of these is a regular term $A(x)$ and the second is a term proportional to a delta function $K\delta(1-x)$. The final term consists of a product of two factors. The first of these is a simple regular function $R(x)$, whilst the second is a function $S(x)$ containing a singular factor $1/(1-x)$ which is regularised by the plus prescription:

$$P(x) = A(x) + K\delta(1-x) + R(x)[S(x)]_+. \tag{A.2}$$

Inserting the form (A.2) into (A.1), we find that the integrals which have to be approximated using the grid have the following general form:

$$I(y) = I_1(y) + I_2(y) + I_3(y) \text{ with} \tag{A.3}$$

$$I_1(y) \equiv \int_x^{1-y} \frac{dz}{z} D(z,y) A\left(\frac{x}{z}\right) \tag{A.4}$$

$$I_2(y) \equiv K D(x,y) \tag{A.5}$$

$$I_3(y) \equiv \int_x^{1-y} \frac{dz}{z} S\left(\frac{x}{z}\right) \left[D(z,y) R\left(\frac{x}{z}\right) - \frac{x}{z} D(x,y) R(1)\right] - R(1) D(x,y) \int_0^{x/(1-y)} dz S(z). \tag{A.6}$$

The integral in the last term of (A.6) can be done analytically for each splitting function. The integrals in (A.4) and the first term of (A.6) are the ones that must be performed on the grid. We note that the integrand in the first term of (A.6) has the property that it is undefined for $z = x$ (due to the fact that $S(x/z)$ contains a factor $1/(1-x/z)$). It nevertheless tends to a finite limit as $z \to x$ (due to the fact that the divergence in $S(x/z)$ is compensated for by the other factor in the integrand going to zero as $z \to x$). This suggests the use of a method for performing the numerical integrations which effectively estimates the integrand between $z = x$ and the grid point with next highest z by extrapolating from integrand values on nearby grid points (with higher z).

A method which uses an open Newton-Cotes rule of degree n for the first n integration intervals, and then switches to a closed Newton-Cotes rule to perform the integration over the remaining intervals, has this property. If the number of integration intervals is greater than 3, we use Simpson's rule as the closed rule, combined with an open rule of degree 4 when the number of integration intervals is even, and an open rule of degree 5 otherwise. Open rules of the appropriate degree are used on their own when the number of intervals is 3 or fewer. This ensures an overall integration method which for most integrals has an

error of $O(n\Delta u^5 \frac{df^{(4)}(\xi)}{du^4})$. In this formula, n is the number of intervals used, Δu is the (even) grid spacing in $u = \ln(\frac{x}{1-x})$, f is the integrand taking into account the Jacobian on the transformation into u space, and ξ is the value of u that maximises $df^{(4)}/du^4$.

With the numerical method described, the integral (A.1) is approximated by:

$$\begin{aligned} I(y) \approx & \sum_{j=i+1}^{k} D(z_j, y) \left[A\left(\frac{z_i}{z_j}\right) + R\left(\frac{z_i}{z_j}\right) S\left(\frac{z_i}{z_j}\right) \right] w_{ijk} \frac{J(z_j)}{z_j} \Delta u \\ & + D(z_i, y) \Bigg[K - R(1) \int_0^{x/(1-y)} dz S(z) \\ & - \sum_{j=i+1}^{k} S\left(\frac{z_i}{z_j}\right) \frac{z_i}{z_j} R(1) w_{ijk} \frac{J(z_j)}{z_j} \Delta u \Bigg]. \end{aligned} \tag{A.7}$$

The indices $\{i, j, k\}$ represent grid points, with i corresponding to the grid point with z value equal to x ($z_i \equiv x$) and k corresponding to the point with z value equal to $1 - y$ ($z_k \equiv 1 - y$). The w_{ijk} are Newton-Cotes type integration weights whose values are dictated by the prescription described above. Note that the weight at grid point j under this prescription depends on the start and end points of the integration – hence w depends on the indices i and k. The function $J(x)$ is the Jacobian, $J(x) \equiv dx/du = x(1 - x)$.

We may rewrite (A.7) as:

$$I(y) \approx \sum_{j=i}^{k} P_{ijk} D(x_j, y), \tag{A.8}$$

where

$$P_{ijk} = \begin{cases} \left[A\left(\frac{z_i}{z_j}\right) + R\left(\frac{z_i}{z_j}\right) S\left(\frac{z_i}{z_j}\right) \right] w_{ijk} \frac{J(z_j)}{z_j} \Delta u & \text{if } i < j \leq k \\ K - R(1) \int_0^{x/(1-y)} dz S(z) & \\ \quad - \sum_{j=i+1}^{k} S\left(\frac{z_i}{z_j}\right) \frac{z_i}{z_j} R(1) w_{ijk} \frac{J(z_j)}{z_j} \Delta u & \text{if } j = i,\ i < k \\ 0 & \text{otherwise.} \end{cases} \tag{A.9}$$

The three-dimensional array P_{ijk} only depends on the splitting function $P(x)$, Jacobian $J(x)$ and weights w_{ijk}. None of these vary during an evolution, with the possible exception of P_{gg} (this contains a term proportional to n_f in the $K\delta(1 - x)$ piece and so may vary in a variable flavour number scheme – see Section 4.2). We therefore precalculate and store the elements of P_{ijk} during program initialisation, to increase efficiency. The possible variation of the contributions to P_{ijk} from the term in P_{gg} proportional to n_f is handled by postponing the calculation of these contributions such that they are calculated and reintroduced at each evolution step (using the value of n_f appropriate to that step).

References

[1] P. V. Landshoff and J. C. Polkinghorne, *Calorimeter triggers for hard collisions*, *Phys. Rev.* **D18** (1978) 3344.

[2] F. Takagi, *Multiple production of quark jets off nuclei*, *Phys. Rev. Lett.* **43** (1979) 1296.

[3] C. Goebel, F. Halzen, and D. M. Scott, *Double Drell-Yan annihilations in hadron collisions: novel tests of the constituent picture*, *Phys. Rev.* **D22** (1980) 2789.

[4] N. Paver and D. Treleani, *Multi - quark scattering and large p(t) jet production in hadronic collisions*, *Nuovo Cim.* **A70** (1982) 215.

[5] B. Humpert, *Are there multi - quark interactions?*, *Phys. Lett.* **B131** (1983) 461.

[6] M. Mekhfi, *Multiparton processes: an application to double Drell- Yan*, *Phys. Rev.* **D32** (1985) 2371.

[7] B. Humpert and R. Odorico, *Multiparton scattering and QCD radiation as sources of four jet events*, *Phys. Lett.* **B154** (1985) 211.

[8] L. Ametller, N. Paver, and D. Treleani, *Possible signature of multiple parton interactions in collider four jet events*, *Phys. Lett.* **B169** (1986) 289.

[9] M. Mekhfi, *Correlations in color and spin in multiparton processes*, *Phys. Rev.* **D32** (1985) 2380.

[10] F. Halzen, P. Hoyer, and W. J. Stirling, *Evidence for multiple parton interactions from the observation of multi - muon events in Drell-Yan experiments*, *Phys. Lett.* **B188** (1987) 375–378.

[11] T. Sjostrand and M. van Zijl, *A Multiple Interaction Model for the Event Structure in Hadron Collisions*, *Phys. Rev.* **D36** (1987) 2019.

[12] M. L. Mangano, *Four Jet Production at the Tevatron Collider*, *Z. Phys.* **C42** (1989) 331.

[13] R. M. Godbole, S. Gupta, and J. Lindfors, *Double parton scattering contribution to W + jets*, *Z. Phys.* **C47** (1990) 69–74.

[14] M. Drees and T. Han, *Signals for double parton scattering at the Fermilab Tevatron*, *Phys. Rev. Lett.* **77** (1996) 4142–4145, [hep-ph/9605430].

[15] G. Calucci and D. Treleani, *Double parton scatterings in high-energy hadronic collisions*, *Nucl. Phys. Proc. Suppl.* **71** (1999) 392–399, [hep-ph/9711225].

[16] G. Calucci and D. Treleani, *Proton structure in transverse space and the effective cross-section*, *Phys. Rev.* **D60** (1999) 054023, [hep-ph/9902479].

[17] **Axial Field Spectrometer** Collaboration, T. Akesson *et. al.*, *Double parton scattering in pp collisions at* $\sqrt{s} = 63\,GeV$, *Z. Phys.* **C34** (1987) 163.

[18] **CDF** Collaboration, F. Abe *et. al.*, *Double parton scattering in* $\bar{p}p$ *collisions at* $\sqrt{s} = 1.8\,TeV$, *Phys. Rev.* **D56** (1997) 3811–3832.

[19] **D0** Collaboration, *Double parton interactions in* γ *+ 3 jet events in* $p\bar{p}$ *collisions at* $\sqrt{s} = 1.96$ *TeV in D0*, *D0 Conference Note 5910-CONF* (2009). Available at http://www-d0.fnal.gov/Run2Physics/WWW/results/prelim/QCD/Q13/Q13.pdf.

[20] A. Del Fabbro and D. Treleani, *A double parton scattering background to Higgs boson production at the LHC*, *Phys. Rev.* **D61** (2000) 077502, [hep-ph/9911358].

[21] A. Del Fabbro and D. Treleani, *Double parton scatterings in b-quark pairs production at the LHC*, *Phys. Rev.* **D66** (2002) 074012, [hep-ph/0207311].

[22] M. Y. Hussein, *A double parton scattering background to associate WH and ZH production at the LHC*, *Nucl. Phys. Proc. Suppl.* **174** (2007) 55–58, [hep-ph/0610207].

[23] M. Y. Hussein, *Double parton scattering in associate Higgs boson production with bottom quarks at hadron colliders*, arXiv:0710.0203.

[24] A. Kulesza and W. J. Stirling, *Like sign W boson production at the LHC as a probe of double parton scattering*, *Phys. Lett.* **B475** (2000) 168–175, [hep-ph/9912232].

[25] E. Maina, *Multiple Parton Interactions, top–antitop and W+4j production at the LHC*, *JHEP* **04** (2009) 098, [arXiv:0904.2682].

[26] E. Maina, *Multiple Parton Interactions in Z+4j, $W^{\pm}$ $W^{\pm}$ +0/2j and W^{+} W^{-} +2j production at the LHC*, *JHEP* **09** (2009) 081, [arXiv:0909.1586].

[27] T. Sjostrand and P. Z. Skands, *Multiple interactions and the structure of beam remnants*, *JHEP* **03** (2004) 053, [hep-ph/0402078].

[28] M. Bahr, S. Gieseke, and M. H. Seymour, *Simulation of multiple partonic interactions in Herwig++*, *JHEP* **07** (2008) 076, [arXiv:0803.3633].

[29] **CDF** Collaboration, F. Abe *et. al.*, *Measurement of double parton scattering in $\bar{p}p$ collisions at $\sqrt{s} = 1.8$ TeV*, *Phys. Rev. Lett.* **79** (1997) 584–589.

[30] R. Kirschner, *Generalized Lipatov-Altarelli-Parisi equations and jet calculus rules*, *Phys. Lett.* **B84** (1979) 266.

[31] V. P. Shelest, A. M. Snigirev, and G. M. Zinovjev, *Gazing into the multiparton distribution equations in QCD*, *Phys. Lett.* **B113** (1982) 325.

[32] Y. L. Dokshitzer, *Calculation of the Structure Functions for Deep Inelastic Scattering and e^+ e^- Annihilation by Perturbation Theory in Quantum Chromodynamics. (In Russian)*, *Sov. Phys. JETP* **46** (1977) 641–653.

[33] V. N. Gribov and L. N. Lipatov, *Deep inelastic e p scattering in perturbation theory*, *Sov. J. Nucl. Phys.* **15** (1972) 438–450.

[34] L. N. Lipatov, *The parton model and perturbation theory*, *Sov. J. Nucl. Phys.* **20** (1975) 94–102.

[35] G. Altarelli and G. Parisi, *Asymptotic Freedom in Parton Language*, *Nucl. Phys.* **B126** (1977) 298.

[36] A. M. Snigirev, *Double parton distributions in the leading logarithm approximation of perturbative QCD*, *Phys. Rev.* **D68** (2003) 114012, [hep-ph/0304172].

[37] E. Cattaruzza, A. Del Fabbro, and D. Treleani, *Fractional momentum correlations in multiple production of W bosons and of $b\bar{b}$ pairs in high energy pp collisions*, *Phys. Rev.* **D72** (2005) 034022, [hep-ph/0507052].

[38] V. L. Korotkikh and A. M. Snigirev, *Double parton correlations versus factorized distributions*, *Phys. Lett.* **B594** (2004) 171–176, [hep-ph/0404155].

[39] A. D. Martin, W. J. Stirling, R. S. Thorne, and G. Watt, *Parton distributions for the LHC*, arXiv:0901.0002.

[40] http://projects.hepforge.org/gsdpdf.

[41] R. K. Ellis, W. J. Stirling, and B. R. Webber, *QCD and Collider Physics*. Cambridge University Press, 1996.

[42] K. Konishi, A. Ukawa, and G. Veneziano, *Jet Calculus: A Simple Algorithm for Resolving QCD Jets*, *Nucl. Phys.* **B157** (1979) 45–107.

[43] K. P. Das and R. C. Hwa, *Quark - anti-Quark Recombination in the Fragmentation Region*, *Phys. Lett.* **B68** (1977) 459.

[44] J. Kuti and V. F. Weisskopf, *Inelastic lepton - nucleon scattering and lepton pair production in the relativistic quark parton model*, *Phys. Rev.* **D4** (1971) 3418–3439.

[45] G. Parisi and R. Petronzio, *On the Breaking of Bjorken Scaling*, *Phys. Lett.* **B62** (1976) 331.

[46] A. I. Vainshtein, V. I. Zakharov, V. A. Novikov, and M. A. Shifman, *Deep Inelastic Lepton Scattering on Hadrons and Gluon Bremsstrahlung*, *JETP Lett.* **24** (1976) 341.

[47] V. A. Novikov, M. A. Shifman, A. I. Vainshtein, and V. I. Zakharov, *Naive Quark Model and Deep Inelastic Scattering*, *Ann. Phys.* **105** (1977) 276.

[48] M. Gluck and E. Reya, *Dynamical Determination of Parton and Gluon Distributions in Quantum Chromodynamics*, *Nucl. Phys.* **B130** (1977) 76.

[49] M. Gluck, R. M. Godbole, and E. Reya, *Dynamically generated parton distributions for high-energy collisions*, *Z. Phys.* **C41** (1989) 667.

[50] M. Gluck, E. Reya, and A. Vogt, *Radiatively generated parton distributions for high-energy collisions*, *Z. Phys.* **C48** (1990) 471–482.

[51] M. Botje, *QCDNUM: Fast QCD Evolution and Convolution*, *ZEUS Note 97-066* (2009). Available at http://www.nikhef.nl/~h24/qcdnum/.

[52] G. P. Salam and J. Rojo, *A Higher Order Perturbative Parton Evolution Toolkit (HOPPET)*, *Comput. Phys. Commun.* **180** (2009) 120–156, [arXiv:0804.3755].

[53] A. Vogt, *Efficient evolution of unpolarized and polarized parton distributions with QCD-PEGASUS*, *Comput. Phys. Commun.* **170** (2005) 65–92, [hep-ph/0408244].